PB-231 992

FEASIBILITY OF A CW LIDAR TECHNIQUE FOR MEASUREMENT OF PLUME OPACITY

Richard A. Ferguson

Stanford Research Institute

Prepared for:

Environmental Protection Agency

November 1973

DISTRIBUTED BY:

NTIS

National Technical Information Service
U. S. DEPARTMENT OF COMMERCE
5285 Port Royal Road, Springfield Va. 22151

BIBLIOGRAPHIC DATA SHEET	1. Report No. EPA-650/2-73-037	2	PB 231 992

4. Title and Subtitle	5. Report Date
FEASIBILITY OF A CW LIDAR TECHNIQUE FOR MEASUREMENT OF PLUME OPACITY	November 1973
	6.
7. Author(s) Richard A. Ferguson	8. Performing Organization Rept. No.
9. Performing Organization Name and Address Stanford Research Institute 333 Ravenswood Avenue Menlo Park, California 94025	10. Project/Task/Work Unit No. 11. Contract/Grant No. EPA 68-02-0543
12. Sponsoring Organization Name and Address EPA, Chemistry and Physics Laboratory National Environmental Research Center Research Triangle Park, North Carolina 27711	13. Type of Report & Period Covered Final Report 14.

15. Supplementary Notes

16. Abstracts

This report describes the work performed for the Environmental Protection Agency during the initial proof-of-concept phase of a program to develop an eyesafe CW lidar for remote measurement of the opacity of smoke plumes from industrial smoke stacks. The analysis, design, construction, and evaluation of a laboratory model CW lidar were performed under SRI Project 1979 from 30 May 1972 to 30 May 1973 under EPA Contract 68-02-0543 to determine the limitations and potential of the technique. The proof-of-principle experiments combine what is called an FM-CW radar technique with an argon laser. The technique involves modulating the intensity of the laser beam at a frequency that changes rapidly and linearly with time. A portion of the transmitted signal is mixed electronically with the light reflected from the targets in a device similar to a radio receiver. Each target appears at a particular frequency. By tuning the radar's receiver to these target frequencies, the researchers were able to measure both the range and the opacity of semi-transparent targets over distances of 100 to 200 meters.

17. Key Words and Document Analysis. 17a. Descriptors

Remote Measurement
Laser
Lidar
Optical Detection
Smoke-Plume Opacity
Measuring Instruments
Air Pollution Monitoring
Smoke Abatement Enforcement

17b. Identifiers/Open-Ended Terms

Air Pollution
Lidar
Clear-Air Scattering
Measuring Instruments

Reproduced by
NATIONAL TECHNICAL
INFORMATION SERVICE
U S Department of Commerce
Springfield VA 22151

17c. COSATI Field/Group 14/02, 20/05, 4/01, 13/02

18. Availability Statement	19. Security Class (This Report)	21. No. of Pages
Release unlimited.	UNCLASSIFIED	96
	20. Security Class (This Page) UNCLASSIFIED	22. Price 8.00 / 1.45

EPA-650/2-73-037

FEASIBILITY OF A CW LIDAR TECHNIQUE FOR MEASUREMENT OF PLUME OPACITY

by

Richard A. Ferguson

Stanford Research Institute
Menlo Park, California 94025

Contract No. 68-02-0543
Program Element No. 1A1010

EPA Project Officer: William D. Conner

Chemistry and Physics Laboratory
National Environmental Research Center
Research Triangle Park, N. C. 27711

Prepared for

OFFICE OF RESEARCH AND DEVELOPMENT
U.S. ENVIRONMENTAL PROTECTION AGENCY
WASHINGTON, D. C. 20460

November 1973

This report has been reviewed by the Environmental Protection Agency and approved for publication. Approval does not signify that the contents necessarily reflect the views and policies of the Agency, nor does mention of trade names or commercial products constitute endorsement or recommendation for use.

Reproduced from best available copy.

SA-1979-27

FRONTISPIECE MODULATED ARGON LASER BEAM TRANSMITTED FROM REMOTE SITE OUT OF VIEW AT LEFT BEING USED TO DETERMINE THE TARGET CHARACTERISTICS OF THE THIN STEAM PLUME RISING FROM BUILDING AT RIGHT

CONTENTS

FRONTISPIECE iii

ABSTRACT v

LIST OF ILLUSTRATIONS ix

ACKNOWLEDGMENTS xi

I INTRODUCTION 1

II SUMMARY AND RECOMMENDATIONS 3

III BACKGROUND 7

IV DESIGN OF THE CW LIDAR 9

A. An Idealized FM-CW Radar 10

B. An Idealized CW Lidar for Opacity Measurement . . . 16

C. A Practical CW Laser Radar 22

1. Laser-Beam Modulation 23

a. Modulation Waveform 23
b. Modulation Techniques 39
c. Modulation Equipment 44

2. Laser Transmitter 47
3. Optical Receiver 51
4. Atmospheric Effects 57
5. Signal Processing 61

V EXPERIMENTAL PROGRAM 65

A. Design and Construction of a Laboratory-Model CW Lidar 65

B. Target Display Characteristics 69

1. Discrete Targets 71
2. Steam-Plume Characteristics 74
3. Clear-Air Targets 77

C. Remote Opacity Measurements 81

D. Discussion of Experimental Results. 86

REFERENCES. 89

BIBLIOGRAPHIC DATA SHEET

ILLUSTRATIONS

1	Basic FM-CW Radar Performance.	11
2	Multiple-Target Performance of an Ideal FM-CW Radar. . .	13
3	Effect of a Moving Target on FM-CW Radar Performance . .	14
4	Distributed Targets and Changes in Their Attenuation Characteristic	15
5	Doppler Spreading of Distributed-Target Spectrum	17
6	Typical Range Profile on Spectrum Display.	19
7	Signal-Processing Block Diagram.	20
8	Result of Finite Limitations on Linear Sweep	24
9	Mixer Output Spectrum.	28
10	Sideband Envelopes of Target Between Node Ranges	33
11	Inaccuracies in Measuring Relative Power Due to Spurious Sidebands	36
12	FM Sweep Using Triangle Waveform	37
13	Improvement in Target Range Resolution by Increasing Deviation, Δf.	40
14	Optical FM-CW Radar Modulation	41
15	FM-AM-CW Radar Modulation.	43
16	Electrooptical Modulator Performance	45
17	Spatial Integration of Beam Intensity Function by Receiver	54
18	Laboratory Model FM-AM-CW Lidar Equipment Block Diagram.	66
19	Measured Modulator Transmission Characteristic	67
20	Data Displays Used for Remote Target Measurements. . . .	70
21	Lidar Target Range Used for Remote Range and Opacity Measurements	72

22 Discrete-Target Spectra Showing Spurious Sideband Changes with Range 73

23 Rooftop Lidar Site 75

24 Distributed Steam-Plume Target Spectrum. 76

25 CW Lidar Clear-Air Returns 78

26 Effects of Spatial Integration on Signal-to-Noise Ratio of Clear-Air Return. 80

27 Changes in Relative Target Power Levels Caused by Various Target Opacities 82

28 Results of Remote Opacity Measurements Using a CW Lidar. 84

ACKNOWLEDGMENTS

The author would like to thank his associates, D. W. Jackson, D. G. Saraf, J.W.O. Knotts, P. Chancellor, D. E. Arnold, R. Cumming, and L. L. Guild for their valuable assistance in the conception, design, fabrication, testing, and documentation of the instrument described herein. In addition, the support and guidance of Mr. William Conner of the Chemistry and Physics Laboratory at NERC/EPA is greatly appreciated.

I INTRODUCTION

This report presents the results of an experimental study to demonstrate the feasibility of a continuous-wave laser radar (CW lidar) for the remote measurement of smoke-plume opacity. The CW radar technique employed was proposed by D. W. Jackson[1]* in January 1970 as an alternative to the pulsed laser technique reported by W. E. Evans[2] in 1967. The work discussed in this report included the analysis, design, fabrication, and limited field evaluation of a laboratory-model CW lidar. The technical work was conducted under Contract 68-02-0543 with the Environmental Protection Agency (EPA) for the twelve months ending 30 May 1973.

The main thrust of this effort was to demonstrate the CW lidar concept with a working hardware model in order to facilitate development of a low-cost, field-tested, portable smoke-plume opacimeter within three years. A distinct lack of published experimental data on CW laser radar performance in the atmosphere had frustrated earlier efforts to analytically determine the proposed system performance. The experimental work reported here provides the results of investigations into actual system performance, operating characteristics, and remote transmission measurement capability using components available at reasonable cost within the state of the art. These new data demonstrate the feasibility of the CW lidar technique and indicate promising directions for continued development.

---

*References are listed at the end of the report.

II SUMMARY AND RECOMMENDATIONS

A theoretical model was developed for a CW (as opposed to pulsed) laser radar capable of measuring laser radiation scattered back from atmospheric particles at ranges between 150 and 500 meters. The model was then examined in light of practical constraints on implementing the CW lidar technique using a low-cost gas laser and inexpensive high-frequency (HF) electronics.

After a survey of this analytical groundwork, actual lidar components were specified and purchased, and a laboratory-model CW lidar was constructed. Transmitting a continuous green beam of light at 5145 angstroms, the lidar was used in a series of proof-of-principle experiments to demonstrate the CW lidar concept.

The technique involves modulating the intensity of the laser beam at a frequency that changes rapidly and linearly with time. A portion of the transmitted signal is mixed electronically with the light reflected from the targets in a device similar to a radio receiver. Each target appears at a particular frequency. By tuning the radar's receiver to these target frequencies, the operator can measure both the range and the opacity of semitransparent targets over distances of 100 to 200 meters.

The blue-green argon laser beam is safer than the powerful, pulsed beams used in earlier lidar monitoring devices that send out megawatts of peak power in pulses faster than the eye's protective blink reaction. The CW laser radar transmits less than 400 milliwatts of power continuously, and is no more harmful to the eye than headlights or reflected sunlight.

Preceding page blank

Since the argon laser beam is safe and continuously visible, it is easier to align and calibrate the CW system than a pulsed laser radar system. Unlike the data output from a pulsed system, the CW radar measurements can be read directly and continuously at the receiver's output, promising easier operation and more reliable data.

A laser radar offers an accurate method for measuring targets that are more than 80 percent transparent. As smokestack emission control laws grow more stringent, enforcement agencies will need accurate measurements of thinner, semitransparent smoke plumes that may be in violation of the law.

In the effort to facilitate development of a field-portable, low-cost lidar opacimeter within three years, the laboratory model was used successfully in actual outdoor experiments to:

(1) Detect and find range to discrete targets.

(2) Detect and find range to distributed scattering targets such as a steam plume and clear-air volumes.

(3) Make remote measurements of target opacities between 10 percent and 50 percent (using a plate glass reference).

It is concluded that there are no fundamental obstacles to employing the CW lidar technique in the remote measurement of smoke-plume opacity using clear-air volumes as detectable reference targets. The engineering requirements for designing an engineering model of the system have been identified.

It is recommended that in order to provide a useful field-portable instrument for remote stack monitoring, research, and enforcement purposes in the near future, a refined research model should be designed, constructed, and field-tested. This model should employ an improved, low-noise receiver detector and dedicated signal-processing electronics based on the three-AM-radio-receiver concept described herein. These

Since the argon laser beam is safe and continuously visible, it is easier to align and calibrate the CW system than a pulsed laser radar system. Unlike the data output from a pulsed system, the CW radar measurements can be read directly and continuously at the receiver's utput, promising easier operation and more reliable data.

A laser radar offers an accurate method for measuring targets that are more than 80 percent transparent. As smokestack emission control laws grow more stringent, enforcement agencies will need accurate measurements of thinner, semitransparent smoke plumes that may be in violation of the law.

In the effort to facilitate development of a field-portable, low-cost lidar opacimeter within three years, the laboratory model was used successfully in actual outdoor experiments to:

(1) Detect and find range to discrete targets.

(2) Detect and find range to distributed scattering targets such as a steam plume and clear-air volumes.

(3) Make remote measurements of target opacities between 10 percent and 50 percent (using a plate glass reference).

It is concluded that there are no fundamental obstacles to employing the CW lidar technique in the remote measurement of smoke-plume opacity using clear-air volumes as detectable reference targets. The engineering requirements for designing an engineering model of the system have been identified.

It is recommended that in order to provide a useful field-portable instrument for remote stack monitoring, research, and enforcement purposes in the near future, a refined research model should be designed, constructed, and field-tested. This model should employ an improved, low-noise receiver detector and dedicated signal-processing electronics based on the three-AM-radio-receiver concept described herein. These

improvements will facilitate night and even daytime use of laser light backscattered from clear-air volumes as references against which plume opacity may be measured. The design of the research model should include investigations of innovative concepts for providing low-cost system-component functions. The completed model should be transportable for remote field measurements of actual plumes and could be used as a mobile research tool to complement existing pulsed lidars. The component and field-performance data provided by such a model would also serve as a basis for constructing a preproduction prototype of a simple, low-cost remote monitoring device for routine enforcement purposes.

III BACKGROUND

Remote measurement of the density of a smoke plume is an important capability in the field of air pollution research and control.[2-8] The single-beam lidar transmission technique has been judged a useful and appropriate means for remote measurement of stack-effluent opacity. The technique's comparison of optical-wavelength power backscattered from "clear-air" regions surrounding a plume is similar to other existing methods using the transmission of visible light to infer particulate concentrations.[2,7-8]

However, lidar developments to date have employed pulsed lasers in systems similar to that described by Evans.[2] These pulsed lidars have certain drawbacks resulting from the transient and high-peak-power characteristics generic to pulsed radars. A relatively expensive pulsed laser with high transmitted power is needed to obtain the necessary signal levels from the backscatter phenomenon. The powerful pulsed beam also presents a potential eye hazard, and precautions must be taken in the design of the lidar to prevent operators or bystanders from looking into the beam. Anyone looking into the beam risks receiving a damaging dose of light energy to the retina since the laser pulse is much faster than the eye's protective blink reaction.

An additional limitation on the pulsed lidar technique is that, because of the transient nature of the low-repetition-rate pulsed lidar echo, data must be recorded on videotape, videodisk, or Polaroid film. Each of these media makes for a somewhat tedious and tardy extraction of opacity values or Ringelmann ratings from the data. While it is now possible to record the transient echo digitally and to analyze the data

Preceding page blank

nearly in real time with a minicomputer, the expense of fielding a practical network of these digital pulsed systems is probably prohibitive.

Drawing on the pulsed-lidar experience of associates at SRI, D. W. Jackson proposed eliminating the transient, high-peak-power drawbacks of pulsed lidars by employing a CW radar technique.[1] Since radar theory shows that the information obtained from a target is a function of average radiated power, a one-watt CW laser could in theory make measurements equivalent to those made by a 50-megawatt pulsed laser transmitting one 20-nanosecond pulse per second. A CW lidar holds promise of greater eye safety, lower cost, and easier operation. A dearth of applicable published data on CW lidar experiments led to the conclusion that a laboratory model should be built to determine the requirements and potential for designing a field-portable CW lidar for remote measurement of smoke-plume opacity. The EPA made funds available for this initial work beginning in May 1972.

IV DESIGN OF THE CW LIDAR

Designing a CW laser radar requires an understanding of CW-radar principles, a practical technique for applying those principles to a laser's optical carrier frequency, and knowledge of the effects on the system due to actual target characteristics and practical limitations on component performance. Section IV-A below satisfies the first requirement by briefly analyzing the idealized frequency-modulated continuous-wave (FM-CW) radar models useful in understanding the lidar design presented later. The adequacy of these models has been amply demonstrated in practice with existing VHF and UHF CW radars. Next, an idealized lidar for measurement of smoke-plume opacity is described in Section IV-B; with this lidar, HF CW radar signals are used to modulate the intensity of the optical carrier. This modulation technique neatly sidesteps the significant problems of optical-frequency modulation, coherent mixing, and holographic signal processing, while making atmospheric aerosol particles visible to a radar employing only existing, low-cost HF electronics technology. Finally, without resorting to rigorous and cumbersome mathematics, the effects of particulate targets and practical component limitations are illustrated with diagrams, simple formulas, and examples drawn from the working model built during this study. The elements of Section IV-C form a basis for designing a low-cost, portable, eye-safe lidar for the remote measurement of smoke-plume opacity. The actual design and performance of a "proof-of-concept" CW lidar opacimeter are discussed in later sections.

A. An Idealized FM-CW Radar

The FM-CW radar employs a frequency-modulated continuous carrier signal to provide range measurement.* If the transmitted frequency f_o is a linear function of time, the range (transit time) to a target is proportional to the difference (or beat) frequency, f_R, between the echo signal and the transmitter signal. A block diagram of the simplest FM-CW radar is shown in Figure 1(a), while 1(b) and 1(c) indicate the idealized relationships between the transmitted frequency, the echo frequency, and the difference frequency as functions of time.

Figure 1(d) shows the frequency spectrum F_R of the output of the mixer used to obtain the difference frequency f_{R1} representing the range R1 to a discrete stationary target placed in the radar's field of view.† Just as a single target appears as a "blip" on the amplitude-vs.-time display of a pulsed radar, the FM-CW radar target appears as a blip on a spectrum analyzer's amplitude-vs.-frequency display of F_R. The target appears as a frequency-component spike at f_{R1}. The reader should note here that if the FM sweep function in Figure 1(b) is not perfectly linear, the difference function f_R does not have a constant value during the sweep. Should the target cross section increase, the delayed FM echo signal received at the mixer input increases, and so does the amplitude of the output of this idealized mixer. The open-bar component in Figure 1(d) represents this increase in the mixer output signal appearing in the spectrum display of F_R.

---

*In principle, the carrier can be either the optical wave itself or a radio-frequency sinusoid that modulates the intensity of the optical wave. For reasons that will be developed later, the latter method was used in our experimental work. However, the present discussion is general and applies to either method.

†The capital letter F_R is used to refer to the entire beat-frequency spectrum of any signals appearing at the mixer output. The lower-case f_R refers to one component in that spectrum.

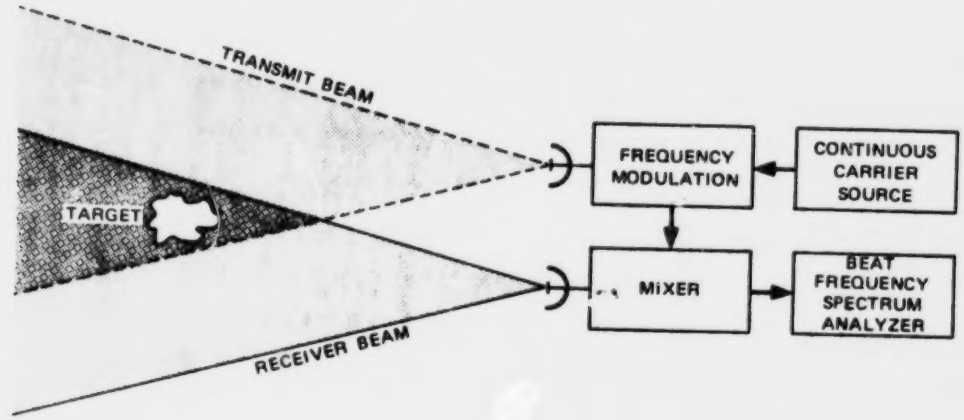

(a) BASIC FM-CW RADAR

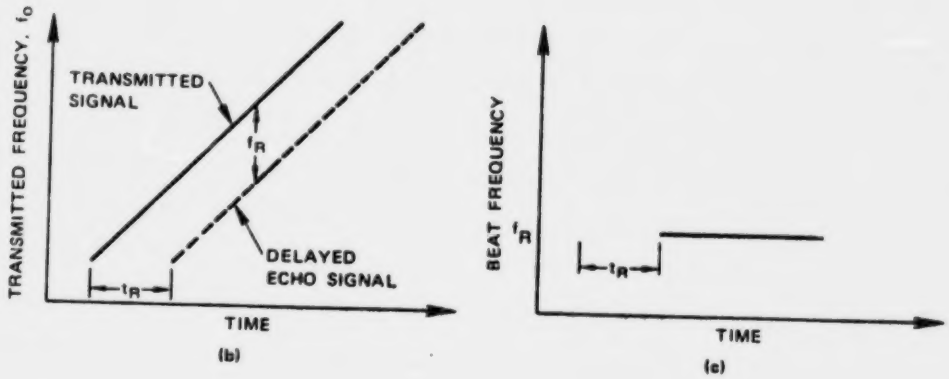

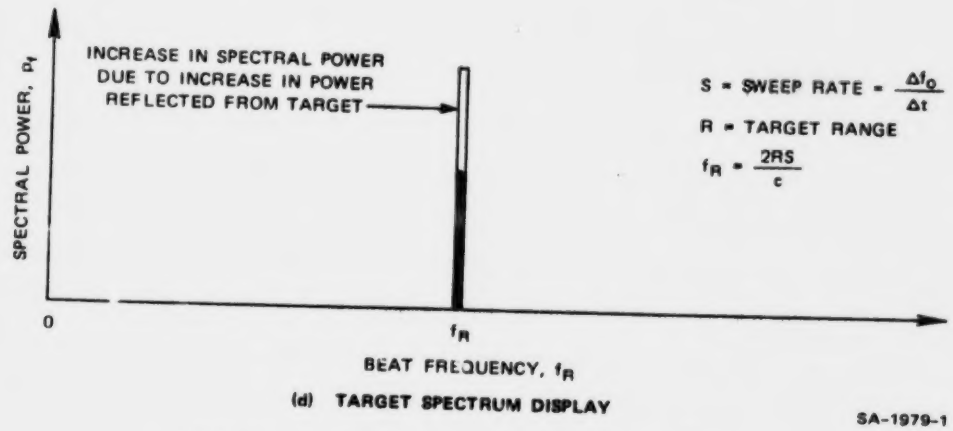
SPECTRAL POWER, P_f
INCREASE IN SPECTRAL POWER DUE TO INCREASE IN POWER REFLECTED FROM TARGET
S = SWEEP RATE = $\frac{\Delta f_0}{\Delta t}$
R = TARGET RANGE
$f_R = \frac{2RS}{c}$
0
f_R
BEAT FREQUENCY, f_R

(d) TARGET SPECTRUM DISPLAY

SA-1979-1

FIGURE 1 BASIC FM-CW RADAR PERFORMANCE

Where two or more targets of varying cross section lie at different ranges in the radar's field of view, superposition theory demands that their echo signal amplitudes add linearly at the mixer input. As a result, the mixer output spectrum will contain two or more Fourier components representing the ranges to the various targets. Figure 2(a) shows the relationship of the multiple delayed echo signals to the transmit signal, while 2(b) presents the resulting mixer output spectrum. Only because the FM sweep function is linear can each of the multiple stationary targets be distinguished as a separate component during the sweep.[1]

Moving targets present still another situation for analysis with the FM-CW radar model. The well known Doppler effect shifts by f_D the frequency of a signal reflected by a target moving at some velocity with a component v along the radar-beam axis. Figure 3(a) shows how an approaching target shifts the echo-signal frequency upward (reducing f_R), while a receding target causes a downward shift in the echo frequency (increasing f_R). The Doppler effects on a spectrum display of f_R are presented in Figure 3(b). Random velocities in a multiple-target situation can cause incorrect range interpretation, as can be seen by comparing the Doppler version of a moving target at R2 [Figure 3(b)] with its stationary range equivalent [Figure 2(b)].

Before leaving the discussion of a simple, idealized FM-CW radar, one more important target situation needs to be considered--multiple scatterers distributed in a volume. Consider first a line of closely spaced stationary targets each of which scatters back some of the transmit-beam energy, causing a characteristic attenuation of the signal with increasing range. Figure 4(a) shows this multiple-target situation on an idealized FM-CW radar-spectrum display of F_R. As the target spacings ΔR_i grow smaller, the corresponding spectral line spacings, Δf_{Ri}, grow

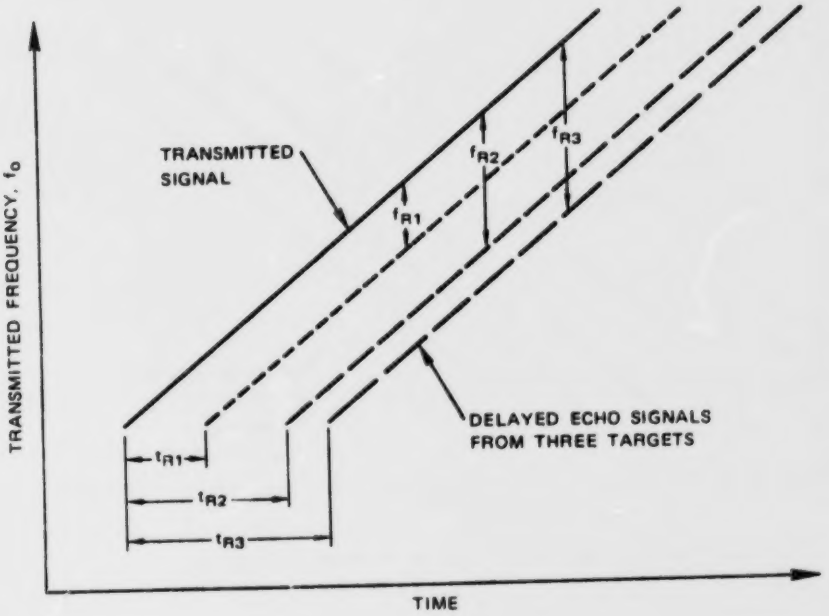

(a) MULTIPLE-TARGET ECHO RELATIONSHIPS TO f_o

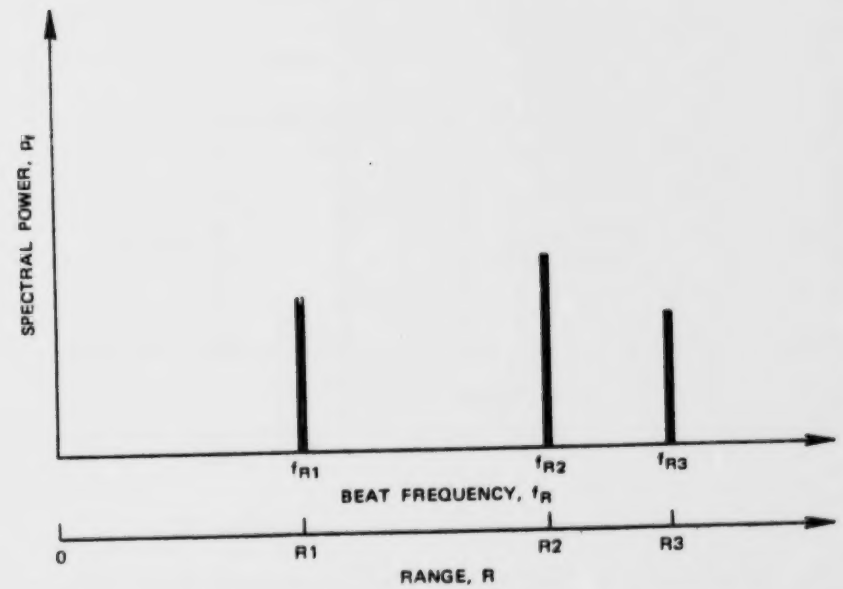

(b) SPECTRUM OF MULTIPLE-TARGET BEAT FREQUENCIES SA-1979-2

FIGURE 2 MULTIPLE-TARGET PERFORMANCE OF AN IDEAL FM-CW RADAR

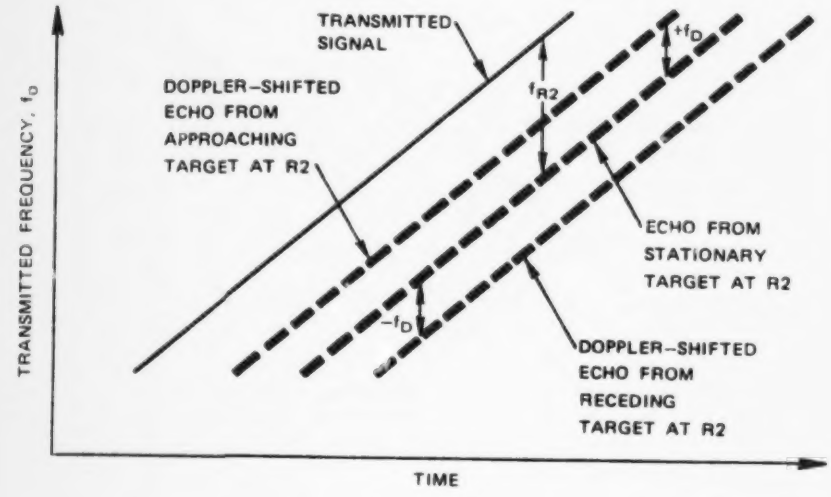

(a) DOPPLER–SHIFTED ECHOES OF TRANSMITTED SIGNAL

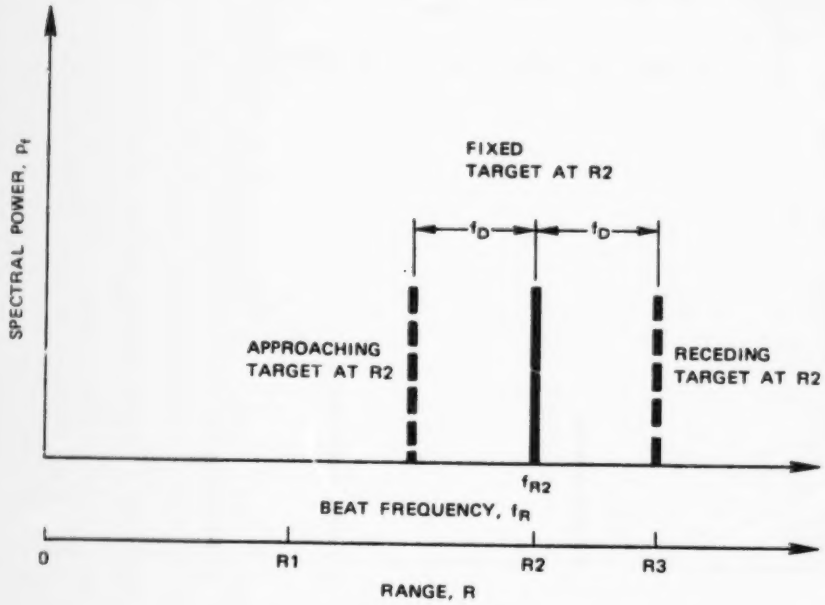

(b) SPECTRUM SHOWING DOPPLER SHIFT FROM CORRECT f_R

SA-1979-3

FIGURE 3 EFFECT OF A MOVING TARGET ON FM–CW RADAR PERFORMANCE

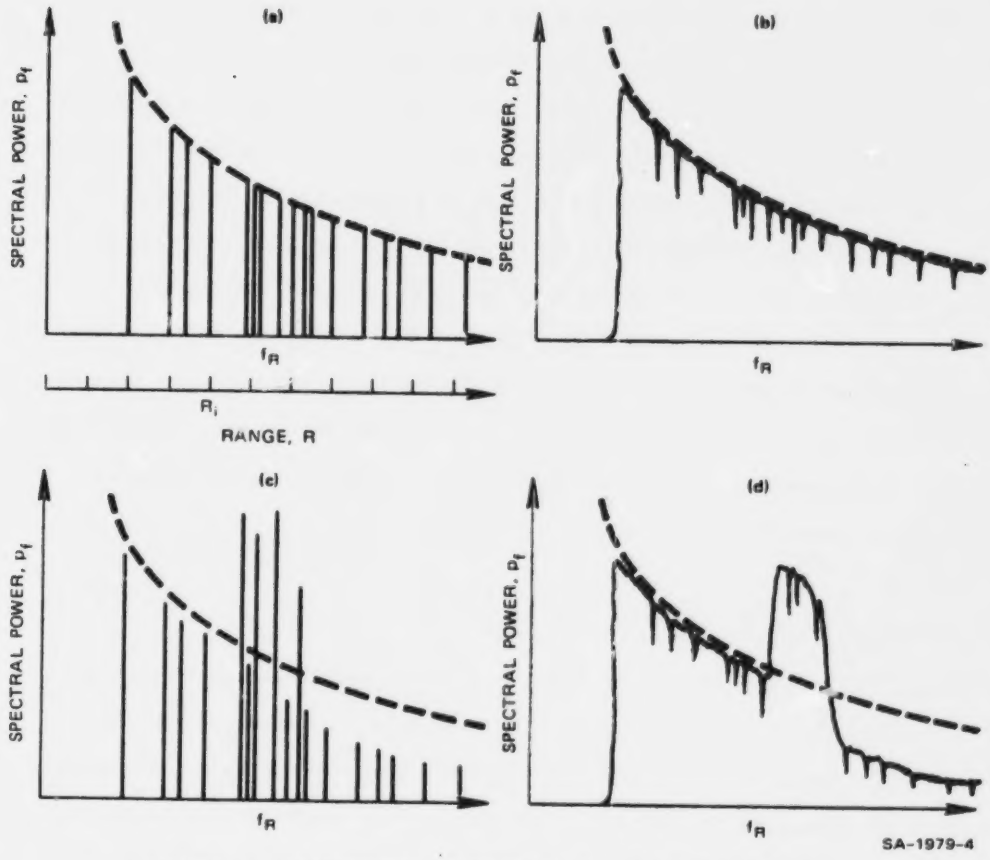

FIGURE 4 DISTRIBUTED TARGETS AND CHANGES IN THEIR ATTENUATION CHARACTERISTIC

narrower and eventually the spectrum display becomes a continuum [Figure 4(b)].

A more complex but appropriate volume target model consists of the same randomly distributed targets shown in Figures 4(a) and 4(b), but includes a cluster of more reflective targets (of higher cross section) in the midst of the original targets. Figures 4(c) and 4(d) demonstrate how the new targets rob transmitted power, causing the attenuation characteristic of the smaller targets to change for ranges beyond that of the new cluster.

Where the distributed target consists of moving elements, Doppler spreading of spectral lines becomes an important consideration. If the various random target velocities are small, with some approaching while others recede, the lines will not shift far and their attenuation characteristic will still be apparent as shown in Figure 5(a). However, if the velocities are high enough, the random shifts f_{Di} up and down can spread the f_R component lines far enough to seriously distort the targets' attenuation characteristic as a function of range [Figure 5(b)]. Since the determination of the attenuation characteristic of multiple scatterers distributed in a volume is the key to adapting an FM-CW laser radar for opacity measurements, the magnitude of Doppler spreading of spectral lines is an important consideration.

B. An Idealized CW Lidar for Opacity Measurement

The FM-CW radar technique idealized above can be extended for use with a CW laser to model an FM-CW lidar capable of making remote transmission measurements on smoke plumes. The use of HF-CW radar modulation signals to modulate the intensity of the optical carrier, and a photodiode device to detect the HF envelope on the received echo, permits existing HF radar electronic signal-processing designs to measure optical power reflected from various ranges. The approach lends itself well to the opacity-measurement problem. Since the optical carrier wavelength is on the order of the particle size or shorter, the amount of radar power backscattered from either "clear-air" particles or plume particles can be great enough for detection. Measurement of the backscatter from particles in volumes at particular ranges can be made simply by examining the spectral power (or amplitude) of the HF mixer output components at the appropriate range frequencies f_R. Transmission can then be determined by comparing laser power backscattered by volumes in front of and behind a semitransparent target.

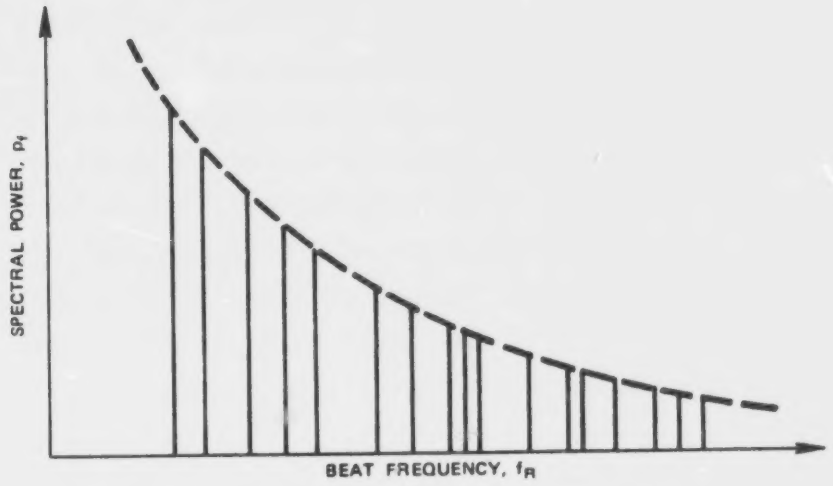

(a) RANDOMLY DISTRIBUTED MULTIPLE TARGETS

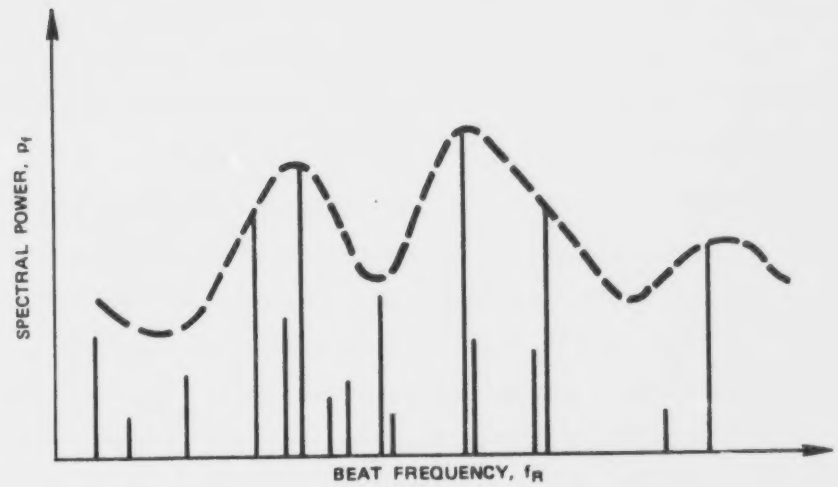

(b) SAME COMPONENTS AS IN (a) SHOWN RANDOMLY DOPPLER-SHIFTED.
Note loss of attenuation characteristic information.

SA-1979-5

FIGURE 5 DOPPLER SPREADING OF DISTRIBUTED-TARGET SPECTRUM

If the particle velocities v_i are low enough to make their Doppler shifts $f_{Di} \ll \Delta f_{Ri}$, the distributed target modeled in Figures 4(a) through 4(d) can be used to explain the CW-lidar-opacity-measurement technique. Figure 6 shows a typical measurement situation with a plume at R = 300 m. Notice that the attenuation characteristic of the clear-air particles suffers a discontinuity and change in value at the range of the plume and beyond. When the plume particles lie in both the transmitter and receiver lidar-beam paths, the amount of transmitted power reaching the far clear-air region is diminished twice by the transmission of the plume along the round-trip echo path. After the received light power backscattered from the far region, P_{far}, and the power received from a near region in front of the plume, P_{near}, are both measured with and then without plume attenuation, the change in the atmosphere attenuation characteristic can be determined. The advantage of the transmission technique is that the logarithms of the relative power $P_{rel} = P_{far}/P_{near}$ for the plume and no-plume cases can give a direct and uniform measure of plume opacity or Ringelmann number that is independent of sky color or backlighting conditions.

Given a CW lidar with the signal-processing functions shown in Figure 7, an operator would measure smoke-plume opacity according to the following scenario. Training the laser beam on the plume, the operator finds the range to the plume by tuning a simple AM radio receiver through the F_R spectrum until he finds the maximum signal at f_{plume}. Two other identical receivers ganged with this receiver then tune automatically to frequencies f_{near} and f_{far} just off the skirts on either side of the plume frequency. The rms voltage outputs of these two receivers correspond to the light power scattered back by "clear-air" particles at ranges R_{near} and R_{far}. The operator does not have to measure both of the scattered power levels. Instead, envelope-detecting log amplifiers take the logarithms of the P_{near} and P_{far} receiver outputs, which are

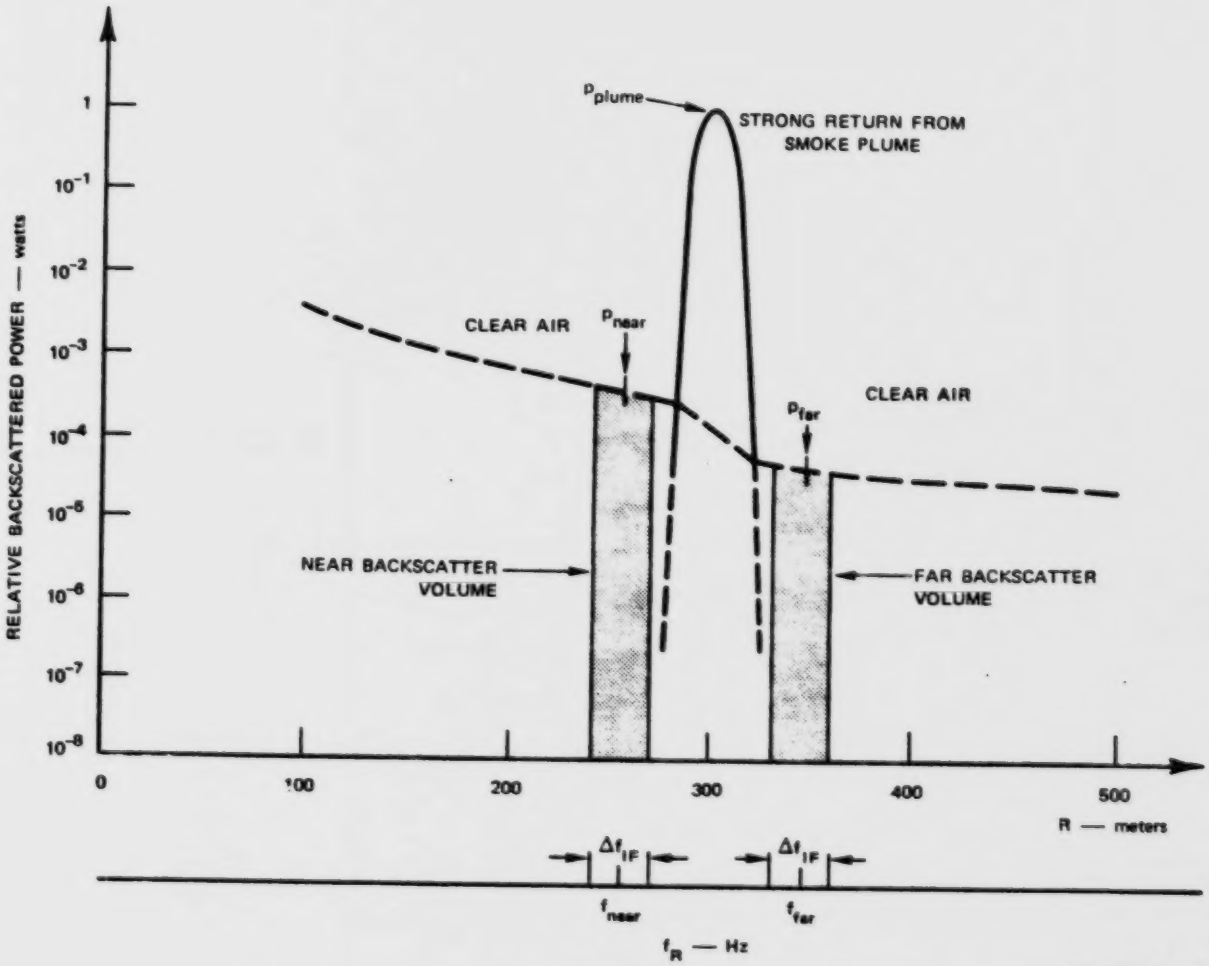

FIGURE 6 TYPICAL RANGE PROFILE ON SPECTRUM DISPLAY

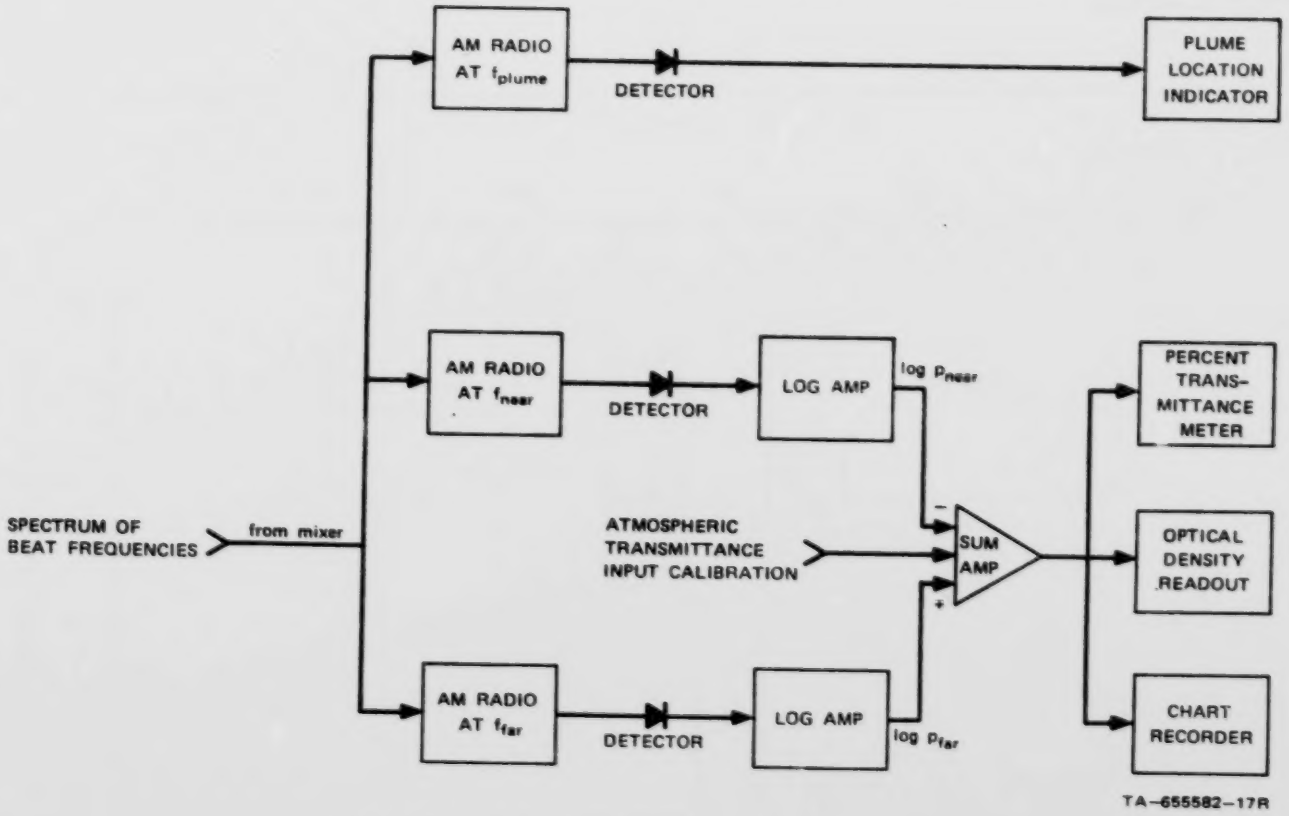

FIGURE 7 SIGNAL-PROCESSING BLOCK DIAGRAM

then subtracted in a difference amplifier. It is the low-bandwidth output voltage of this difference amplifier that can be read at a meter or chart recorder by the operator. But first the operator needs to calibrate the system to compensate for such biasing factors as atmospheric attenuation due to clear-air particles in the plume volume.

The calibration is relatively simple. Once his scattering-volume ranges are selected around the plume, the operator directs the lidar beam through clear air alone slightly to one side of the plume. The output voltage that he reads is simply:

$$v_o = \left[\log P_{near} - \log P_{far}\right]_{\text{no plume}} \qquad (1)$$

$$= \left[-\log P_{rel}\right]_{\text{no plume}} .$$

By adjusting a dc bias control on the differential amplifier, the operator can return the amplifier output to zero. This effectively sets a constant dc baseline shift in the signal-processing device, biasing the output by the amount $[+\log P_{rel}]$ no plume.

Now the operator points his lidar back through the plume and observes the output of the amplifier again:

$$v_o = \left[\log P_{near} - \log P_{far}\right]_{\text{plume}} + \text{dc bias calibration factor}$$

or

$$v_o = -\log\left(P_{rel}\right)_{\text{plume}} + \log\left(P_{rel}\right)_{\text{no plume}}$$

$$v_o = \log\left(P_{rel}\right)_{\text{no plume}} - \log\left(P_{rel}\right)_{\text{plume}} . \qquad (2)$$

Because light signal power scattered from the far volume behind the plume is reduced twice by the transmission T_p of the plume,

$$\left(P_{far}\right)_{plume} = T_p^2\left(P_{far}\right)_{no\ plume} \quad . \tag{3}$$

Thus,

$$v_o = \log\left(\frac{P_{rel}}{T_p^2\, P_{rel}}\right)$$

$$v_o = -\frac{1}{2}\log T_p \quad . \tag{4}$$

This output is directly proportional to the plume's optical density, where optical density is defined for transmission T between zero and 1.0 as (-log T). In short, the idealized CW lidar allows an operator to continuously read the opacity of the plume after a simple calibration of the clear-air return.

C. A Practical CW Laser Radar

The laser radar designer must hurdle a number of practical obstacles to building a working model of the basic CW laser radar discussed in Section IV-A, above. Perhaps the easiest obstacles to define and surmount are those posed by equipment performance limitations such as nonlinearity and bandwidth. More difficult to examine at the design stage are problems for which inadequate design data exist, as is the case in estimating the severity of Doppler effects from the various atmospheric particle velocities. Also, investigations into actual operating characteristics such as ease of data interpretation cannot be made until hardware is built for evaluation.

In this section the reduction of the basic CW laser radar to practice will be discussed under several subheadings, as follows: laser-beam modulation, laser transmitter, atmospheric effects, laser receiver, and signal processing. The intent here is to characterize the practical design problems of a CW lidar. Detailed design data are best included in a later section.

1. Laser-Beam Modulation

The choice of modulation parameters, technique, and equipment is crucial to the performance of a CW lidar. It will be helpful to examine first some important and generally applicable effects of realistic modulation waveform parameters. The discussion of practical ways to put these waveforms on an optical carrier can then more profitably follow.

a. Modulation Waveform

The linear frequency sweep shown in Figure 1(b)--fundamental to the multiple/distributed-target detection capability of the FM-CW radar--cannot be sustained forever. Practical modulators have both upper and lower limits on f_o, as well as maximum sweep rates S and imperfections in sweep linearity. Since the modulated frequency f_o cannot increase indefinitely, at some time it will have to return in some fashion to the desired minimum "start" frequency. The fact that the sweep lasts only for a period T and covers a finite total deviation Δf_o throws an uncertainty into the range measurement.

As is obvious from Figure 8(a), if the target's range delay time t_R is greater than the duration of the sweep T, $f_R(t)$ will be the difference between the transmitted FM signal and whatever frequency content exists at the receiver input prior to the echo return. An equally useless difference function results when the FM echo mixes with the

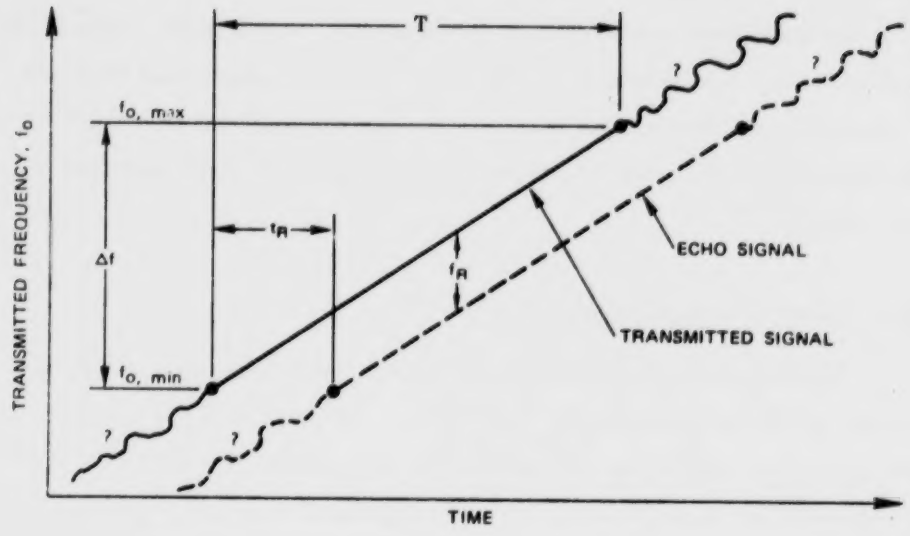

(a)

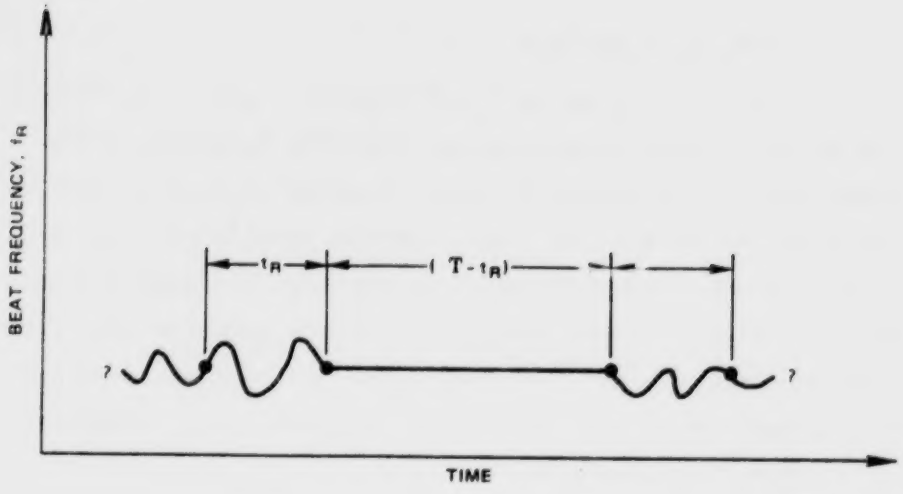

(b)

SA-1979-6

FIGURE 8 RESULT OF FINITE LIMITATIONS ON LINEAR SWEEP

unspecified signal following the transmitted sweep. Sweep duration T must exceed t_R by a margin of a few periods t_R in order to generate a constant value of f_R long enough for signal processing to be completed. For example, a radar useful up to a 500-m range, where $t_R = 3\ \mu s$, will need a linear sweep lasting 10 μs in order to generate 7 μs of constant beat frequency f_R. But if f_R does not complete at least one cycle in the 7 μs, no signal processor can measure the value of f_R during $(T - t_R)$. Moreover, if the signal processor is to discriminate between a change in f_R and an arbitrary uncertainty Δf_R in measuring f_R, at least one cycle of Δf_R must also be completed during $(T - t_R)$ as well. Thus three practical design constraints result from sweep-duration considerations:

$$T \gg t_R \text{ (where } t_R \text{ is the maximum value expected)} \tag{5a}$$

$$T \geq 1/f_R + t_R \tag{5b}$$

$$T \geq 1/\Delta f_R + t_R \quad . \tag{5c}$$

In order to apply these constraints to achieve desired range resolution, the sweep extent, or total deviation Δf_o, must be considered.

We can define the difference frequency f_R from the parameters listed in Figure 8(b). For a linear sweep rate S lasting T seconds, where $\Delta f_o = ST$, f_R is equal to the frequency change that occurs during transit time t_R, or

$$f_R = St_R \quad . \tag{6}$$

Since

$$t_R = 2R/c \quad ,$$

then

$$f_R = \frac{2RS}{c} \tag{7a}$$

or

$$f_R = \frac{2R\Delta f_o}{cT} \quad . \tag{7b}$$

Solving for range R:

$$R = \frac{cf_R T}{2\Delta f_o} \quad . \tag{8}$$

The uncertainty in range (ΔR) is related to the uncertainty in difference frequency (Δf_R) by

$$\Delta R = \frac{c\Delta f_R T}{2\Delta f_o} \tag{9}$$

and recalling that

$$T \geq \frac{1}{\Delta f_R} \quad ,$$

it follows that

$$\Delta R \geq \frac{c}{2\Delta f_o} \tag{10}$$

and

$$\Delta f_o \geq \frac{c}{2\Delta R} \quad . \tag{11}$$

Equation (10) shows that range uncertainty is a function only of the maximum deviation Δf_o achievable in a sweep time T.

The foregoing analysis applies to measurement consisting of a single sweep through Δf_o in time T. As in the example above, T needs to be only a few tens of microseconds in order to meet the constraint posed by the maximum 3-μs transit time to a target at 500 meters. Laser modulators such as that used in this study can readily achieve a linear sweep through a Δf_o of 5 MHz in 100 μs. From the above expression for uncertainty ΔR in terms of Δf_o it follows that one sweep through a 5-MHz deviation gives a 30-meter range uncertainty. However, if a large number, n, of 5-MHz sweeps can be made, a signal processor can make an improved measurement of beat frequency f_R during the extended period nT, and thereby reduce the uncertainty in R.

Generating repeated sweeps where Δf_o cannot extend above some practical limit $f_{o,max}$ requires that f_o be reset at the end of one sweep. Figure 9(a) shows one obvious way of obtaining a series of n single-sweep measurements of f_R. The adjoining plot of f_R versus time for a single-target situation [Figure 9(b)] shows that this sawtooth FM waveform repeated at some modulation frequency f_m gives a relatively constant output value f_R, with a short burst of error frequency $f_e(t)$ occurring every $T_m = 1/f_m$. Since there is a finite reset or turnaround time t_t at the end of the sweep, this periodic deviation from the constant f_R value lasts for a period $t_d = t_R + t_t$. Just as sweep duration T was constrained to be longer than t_R by at least $1/\Delta f_R$ [Eq. (5c)], so T must be reconstrained in the repetitive sweep situation as follows:

$$T \geq t_d + 1/\Delta f_R \qquad (12a)$$

$$T \geq t_d + 1/f_R \quad . \qquad (12b)$$

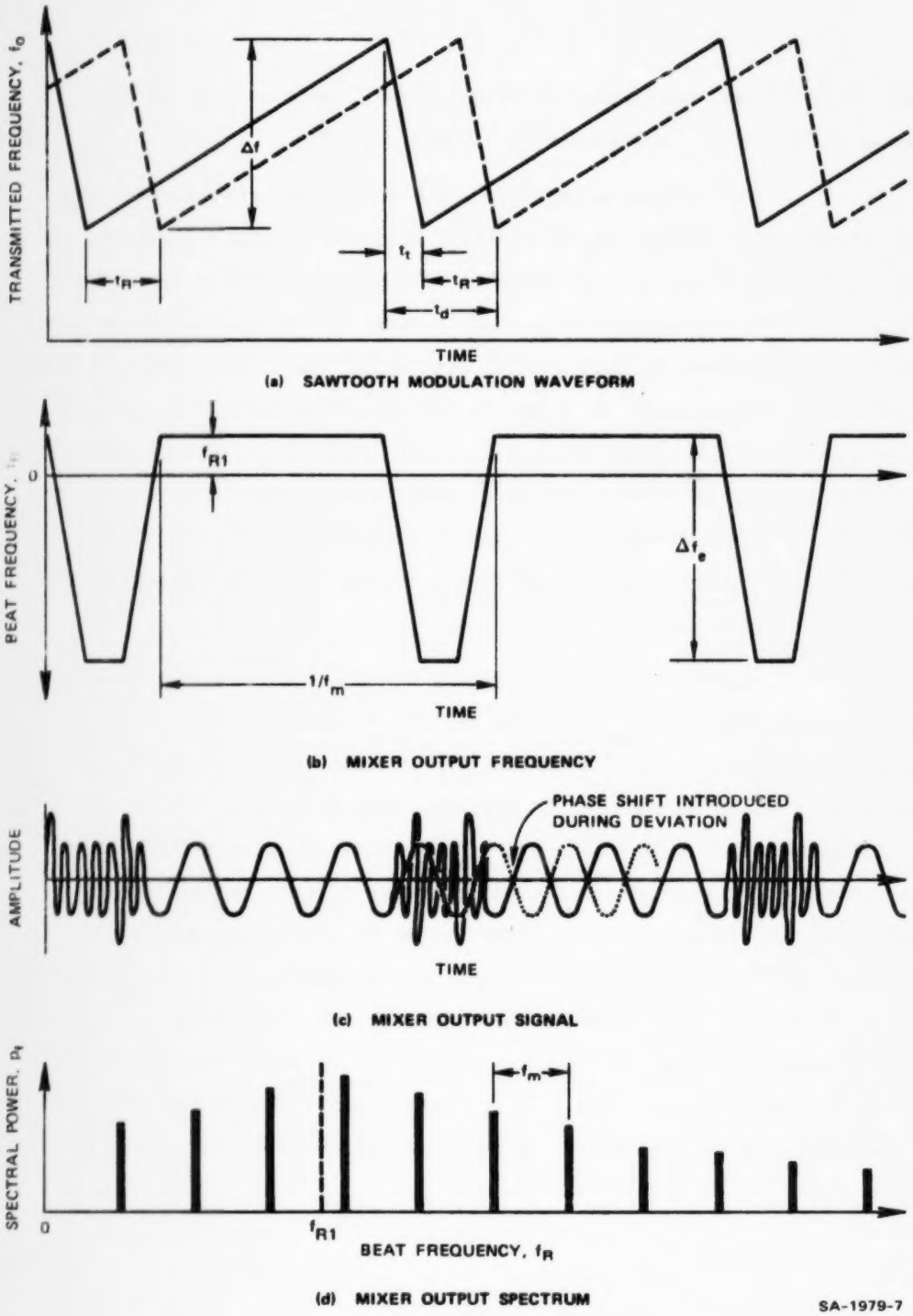

FIGURE 9 MIXER OUTPUT SPECTRUM

The periodic deviation in f_R has a much more profound effect on the design of a practical FM-CW lidar than this time constraint, however. Notice in Figure 9(b) that $f_R(t)$ is now a frequency-modulated function, deviating some Δf_e at a repetition frequency f_m around an average frequency that can be shown to be $f_c = 0$. Fourier analysis of an FM signal waveform shows that the spectrum contains an infinite number of sideband components separated by f_m and clustered about the average frequency. Figure 9(d) shows such a spectrum for the function f_R corresponding to the single-target situation modeled in Figures 9(a) and 9(b). It is no longer obvious from the spectrum display that a single target is located exactly at R1. Unless it is possible to narrow the envelope of the sidebands around the "true" range frequency f_{R1}, or otherwise eliminate spurious spectral peaks, useful single-target detection would be difficult and multiple-target discrimination impossible.

In designing a practical solution to the sideband problem, it will be helpful to develop an understanding of the sideband spectrum and its causes. A rigorous mathematical analysis is lengthy and is not needed here to define and solve the problem. However, a few key points will be developed mathematically here. Figure 9(c) shows the amplitude-vs.-time plot of the waveform whose frequency $f_R(t)$ changes as in Figure 9(b). Notice the amplitude and frequency irregularity during t_d. Notice that the constant-frequency signal after the deviation does not necessarily pick up in phase with its last value before the discontinuity. It is these amplitude and phase irregularities caused by the periodic deviation at rate f_m that generate the numerous Fourier sideband components.

The spectrum of this frequency-modulated mixer output signal is presented in Figure 9(d). Notice that the spectral power levels of the sidebands have an envelope characteristic. As the nature of the

f_R deviation changes, the modulated signal waveform and its irregularity also change, requiring a new sideband power distribution to generate the new Fourier sum. During this study we found that the factors determining the deviation in $f_R(t)$ can indeed be altered to "improve" the resulting FM spectrum.

The deviation of $f_R(t)$ shown in Figure 9(b) can be characterized by:

- Its duration, $t_d = t_R + t_t$
- Its waveform, $f_e(t)$
- Its repetition rate, f_m
- The initial phase value φ_1 at the start of t_d.

The practical factors controlling t_d are the target range $R = ct_R/2$, and the modulator's bandwidth (or maximum slewing rate), which determines reset time t_t. Factors controlling the form of $f_e(t)$ during the deviation are the extent and linearity of Δf achieved by the sweep rate S during deviation time t_d. The repetition rate of the frequency deviations is equal to the FM sawtooth repetition rate f_m. Finally, the factor determining φ_1 is the duration of the constant frequency f_{R1} up to the start of t_d.

In order to single out a target on the spectrum display of F_R, spurious sideband power must be reduced in such a way as to single out the real target frequency as calculated ideally by Eq. (7):

$$f_{R1} = \frac{2R1\Delta f_o}{cT} \quad .$$

At first glance this appears to be a discouraging task since many controlling parameters do not appear in the idealized equation. Fortunately, several parameters can be combined to give a simpler, approximate but very

useful result showing that Δf_o can be adjusted to minimize sidebands. The dependence of target resolution on Δf_o is borne out in practice as well.

It can be shown that the starting phases of all segments of the mixer output f_{R1} are equal to each other. Hence, for phase coherence and the consequent reduction in spurious sideband levels, it is necessary and sufficient that

$$f_{R1} T_m = n \quad , \tag{13}$$

an integer.

Combining this with Eq. (7) gives

$$\frac{2R1\Delta f_o}{c} \frac{T_m}{T} = n \quad . \tag{14}$$

Under these conditions, there must be just enough time for an integral number of cycles of f_{R1} to occur during the full period T_m, in order for phase to match at the endpoints of each T_m. In other words, for minimum sidebands:

$$T_m/T_{R1} = n \tag{15}$$

where n is an integer and $T_{R1} = 1/f_{R1}$. Since n is also a function of Δf_o [Eq. (14)], a handy design rule is that a single target will best stand out from surrounding sideband components when

$$\Delta f_o \frac{2R1}{c} = n \quad . \tag{16}$$

But this also means that $f_{R1}/f_m = n$ is a condition for minimum sidebands, so that only when Δf_o is adjusted to make f_{R1} a multiple of f_m will a target stand out of its own sideband "noise." A radar operator with a single knob to adjust Δf_o could therefore isolate his target by "detuning" the spurious sidebands with the knob.

Conversely, if Δf_o is fixed along with f_m, there will be several target ranges R_n such that for

$$R_n = \frac{nc}{2\Delta f_o} \tag{17}$$

clean radar target displays will result with no adjustment of Δf. These minimum-sideband ranges can aptly be termed "node ranges," and the spacing between two adjacent node ranges is:

$$\Delta R_n = R_{n+1} - R_n$$

$$= \frac{c}{2\Delta f_o} (n + 1 - n)$$

$$\Delta R_n = \frac{c}{2\Delta f_o} \quad . \tag{18}$$

For a single stationary target between two adjacent node ranges, the sidebands at nf_m are largest for the values of n that make nf_m close to the value of f_R calculated ideally from Eq. (7). The apparent "average" location of these larger sidebands is f_R, and if their envelope characteristic is drawn as in Figure 10(b) the envelope's peak lies at f_{R1}, although no spectral component is found there. As the target moves between node ranges, the larger sideband amplitudes change as if to roll their envelope characteristic along the spectrum with the changing target range (ignoring Doppler effects, of course). When the target reaches a node range where $f_{R_n} = nf_m$, the envelope narrows around

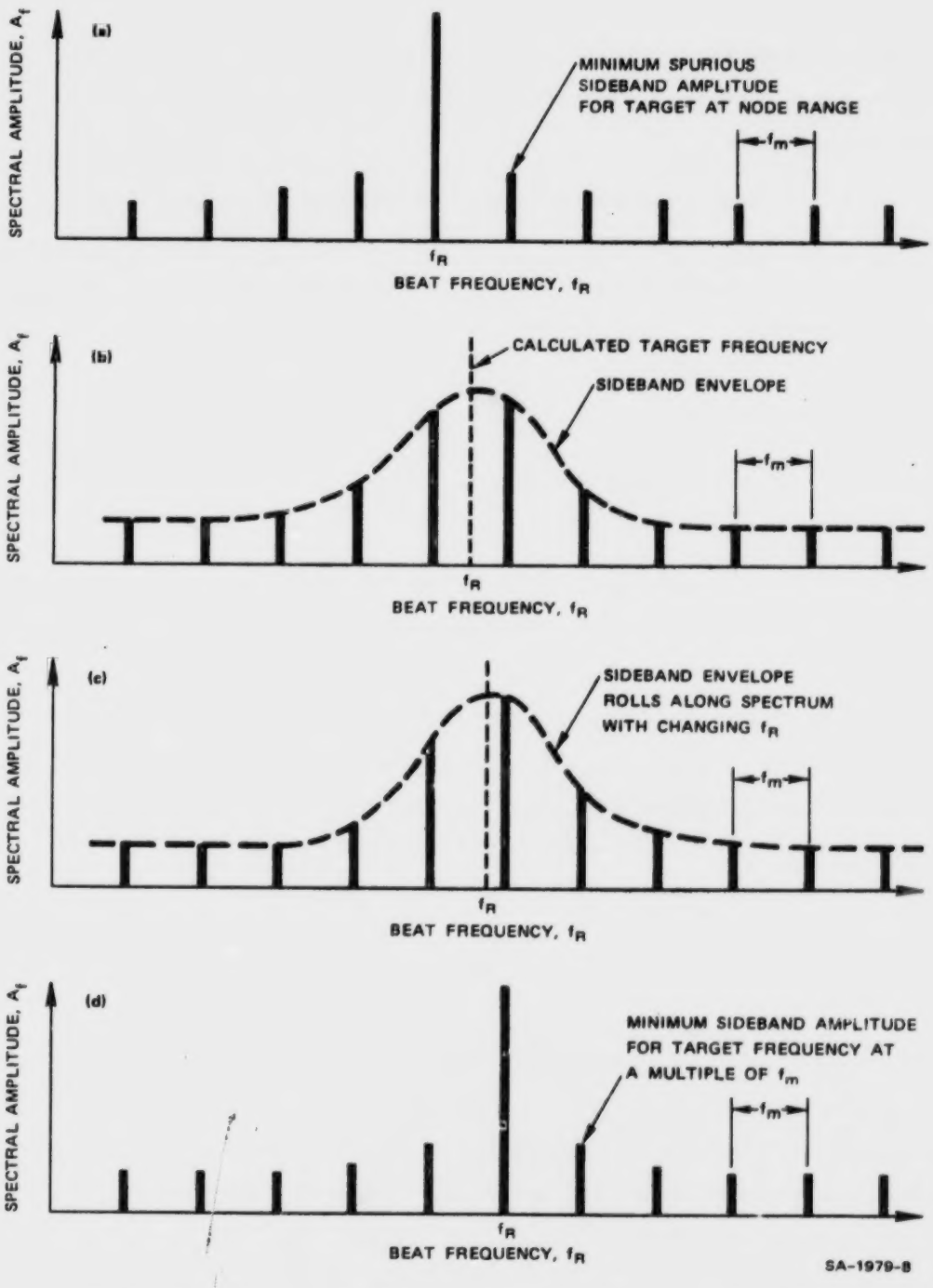

FIGURE 10 SIDEBAND ENVELOPES OF TARGET BETWEEN NODE RANGES

the correct node-range component. This effect is depicted in Figures 10(a) through 10(d). It is instructive to examine range uncertainty in this situation.

Since the sawtooth sweep is repeated and sideband components f_i exist continuously, a sufficiently sophisticated signal processor could measure n of the larger sideband amplitudes, A_i, calculate the product $f_i A_i$, and determine an average range frequency

$$f_R = \frac{\sum_{k}^{k+n} f_i A_i}{\sum_{k}^{k+n} A_i} \qquad (19)$$

which would, for increasing n, get arbitrarily close to the ideal value of f_R resulting from a single continuous sweep during the long measurement time. But to the eye, or to a simple data processor that merely categorizes the target frequency as lying between the two largest sidebands, the uncertainty in range is just the node range spacing $\Delta R_n = c/2\Delta f$. The reader has probably recalled by now the result derived earlier for range uncertainty ΔR in a measurement made during single-sweep T through Δf [Eq. (10)]:

$$\Delta R = c/2\Delta f_o \quad ,$$

which is just the node range spacing for the repetitive-sweep case. It is apparent that, even though the repeated sweep sawtooth makes data available for calculating accurate f_R, an unsophisticated signal processor may not allow range resolution any better than that possible from a single-sweep measurement.

Another kind of accuracy limitation is also created by the sideband noise. Recall the intensity-modulation technique assumed here. The amount of power reflected back by a single target is proportional to laser-beam intensity, and is therefore proportional to the amplitude (not power) of the HF radar signals that modulate the optical-carrier intensity and are returning from the target range. Thus it is a display of spectral-component amplitude that gives a direct measure of received laser power reflected by targets at various ranges. Now, if two targets lie in the lidar's field of view, the sidebands of one will add to the main component of the other, making it difficult to determine accurately the ratio between the two target power levels. Figure 11 shows how such an inaccuracy develops. It should also be obvious that the inaccuracy is minimized when spurious sideband levels are lowest--namely, when the discrete targets are located at node ranges.

It was at these node ranges, for example, that discrete, semitransparent targets were placed in this experimental study to demonstrate the remote opacity-measurement capability of an FM-CW lidar, as discussed in Section V. In practice, spurious-component amplitudes could be reduced to between 5 and 10 percent of the main node-range component. In an effort to improve upon this by further reducing sideband levels, another kind of sweep waveform was investigated--the triangle wave.

The desired effect of the triangle-wave sweep is to reduce the duration of the error-frequency burst $f_e(t)$ during t_d (Figure 12). Moreover, since the sweep function during turnaround time t_t is symmetric in every respect with the function during the basic sweep time T, the value of $f_e(t)$ during t_t is just

$$f_e\left(t_t\right) = -f_R \quad . \tag{20}$$

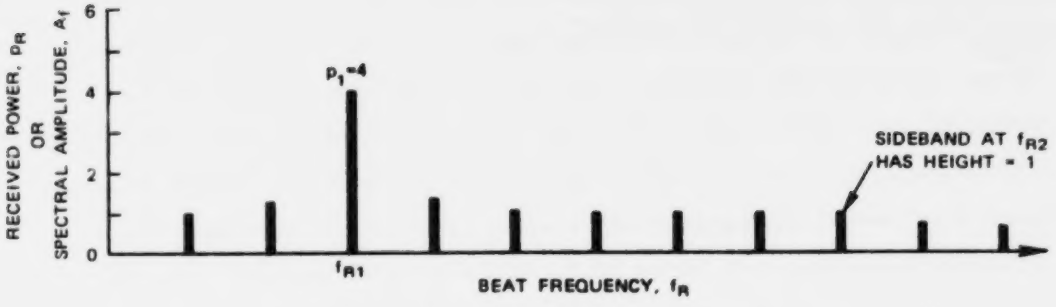

(a) TARGET AT R1 REFLECTS FOUR UNITS OF OPTICAL POWER

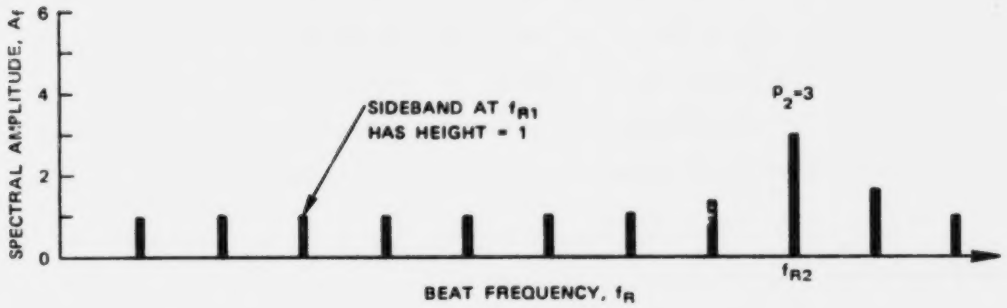

(b) TARGET AT R2 REFLECTS THREE UNITS OF OPTICAL POWER

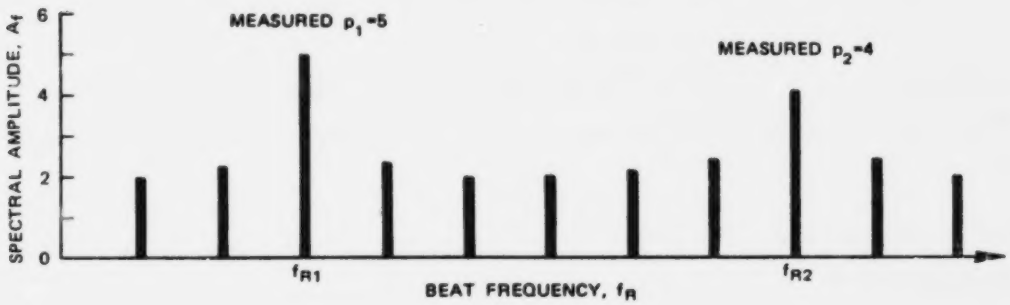

(c) TWO TARGETS ABOVE VIEWED TOGETHER BY FM-CW RADAR
Measured value of $p_{relative} = p_1/p_2 = 1.25$ instead of actual value of 1.33

SA-1979-9

FIGURE 11 INACCURACIES IN MEASURING RELATIVE POWER DUE TO SPURIOUS SIDEBANDS

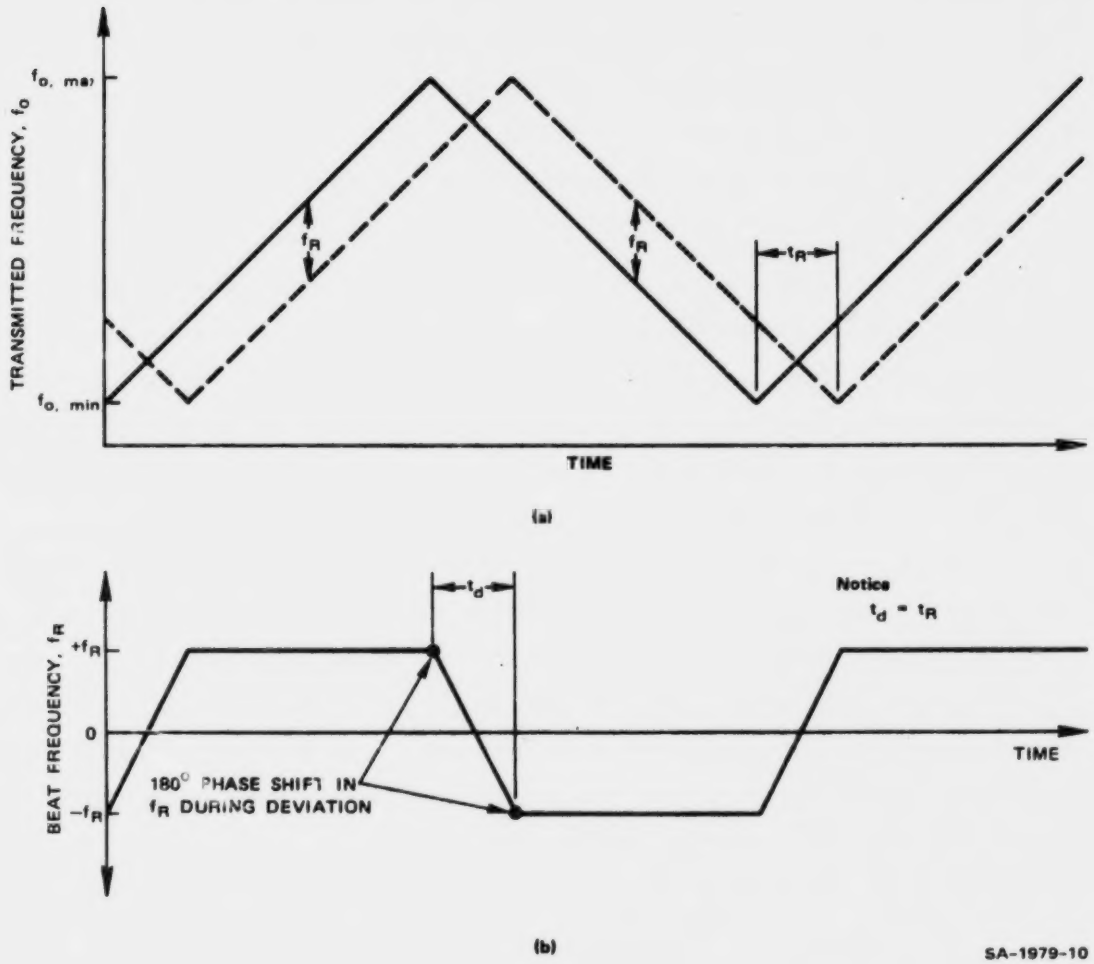

FIGURE 12 FM SWEEP USING TRIANGLE WAVEFORM

In this case $f_R(t)$ is either a constant $+f_R$ or $-f_R$ except during the remaining deviation time t_R. A sweep rate during t_t equal to the sweep rate during T apparently reduces the undesired effects of bandwidth or slewing limitations that occur in a practical sawtooth modulator due to its rapid reset time. A linear sweep produces the desired constant value $|f_R|$ for a larger fraction of the repetition period T_m in a triangle wave than in a sawtooth waveform. Indeed, in practice the spurious sidebands generated in a real mixer output by triangle-wave modulation could often be reduced to as little as 3 percent of the amplitude of the main node-range frequency component.

It can be shown that the triangle-wave sweep unfortunately introduces a strong dependence on f_{oc}, the center frequency of the transmitted frequency sweep (Figure 12). Up to now, f_{oc} did not figure significantly in the analysis or performance. Suffice it to say here that because triangle-wave measurement of $|f_R|$ is made during both its positive and its negative phases, the 180° phase shift it undergoes during the deviation period must enter into the calculation of phase-coherence conditions leading to Eq. (13). These values in turn define the conditions for minimum sideband power. A designer may choose to accept the f_{oc} dependence in order to gain a few percent in the sideband reduction. He should, however, be prepared to deal with the f_{oc} sensitivity in calibrating and operating the lidar. The sensitivity to this parameter greatly reduces the number of practical combinations of Δf and f_m that can be "tuned in" by the operator to put a node range at the actual target range.

Both sawtooth and triangle sweep waveforms are suitable for multiple-target situations where each discrete target is spaced several node ranges away from its nearest neighbor. However, closer target spacings would cause one target's sideband envelope to overlap the other target's envelope, making it difficult both to resolve the two targets

and to measure their relative reflected power levels accurately. Where one target reflects 20 to 100 times the power of another, its sidebands alone could dwarf the main component of the weaker target. Given a minimum target spacing, ΔR_{min}, one might attempt to improve target resolution by increasing Δf_o until range node spacing, $\Delta R_n = c/2\Delta f_o$, is narrowed to a fraction of ΔR_{min}. Eventually the practical limit on Δf_o will be reached and no further sideband envelope narrowing can be achieved (Figure 13). If at this point, $\Delta R_n > \Delta R_{min}$, the multiple-target range profile becomes inaccurate unless other steps can be taken to reduce the spurious sideband component levels.

b. Modulation Techniques

Once an appropriate sweep modulation waveform has been chosen, the techniques for applying the waveform to the optical-wavelength carrier must be specified. There are two alternative design routes: (1) modulate the optical frequency (color) of the transmitted laser beam itself, or (2) modulate a lower subcarrier center frequency that in turn is used to modulate the intensity of the laser beam.

The necessary prerequisite for optical-frequency modulation is a tunable laser transmitter (see Figure 14). In the visible region, such sources are now available, offering Δf greater than tens of gigahertz with single-frequency stabilities of 100 MHz. Modulation is usually accomplished by changing the laser's cavity length, etalon spacing, or end-reflector wavelength. The laser outputs can be swept through large Δf at audio rates by using acoustic or piezoelectric transducers. Such lasers are uniformly expensive, and only very recently have they emerged from the laboratory development stage.[11] The linearity and repeatability of the sweep available from these lasers is difficult to measure and is seldom if ever specified or measured by the manufacturers.

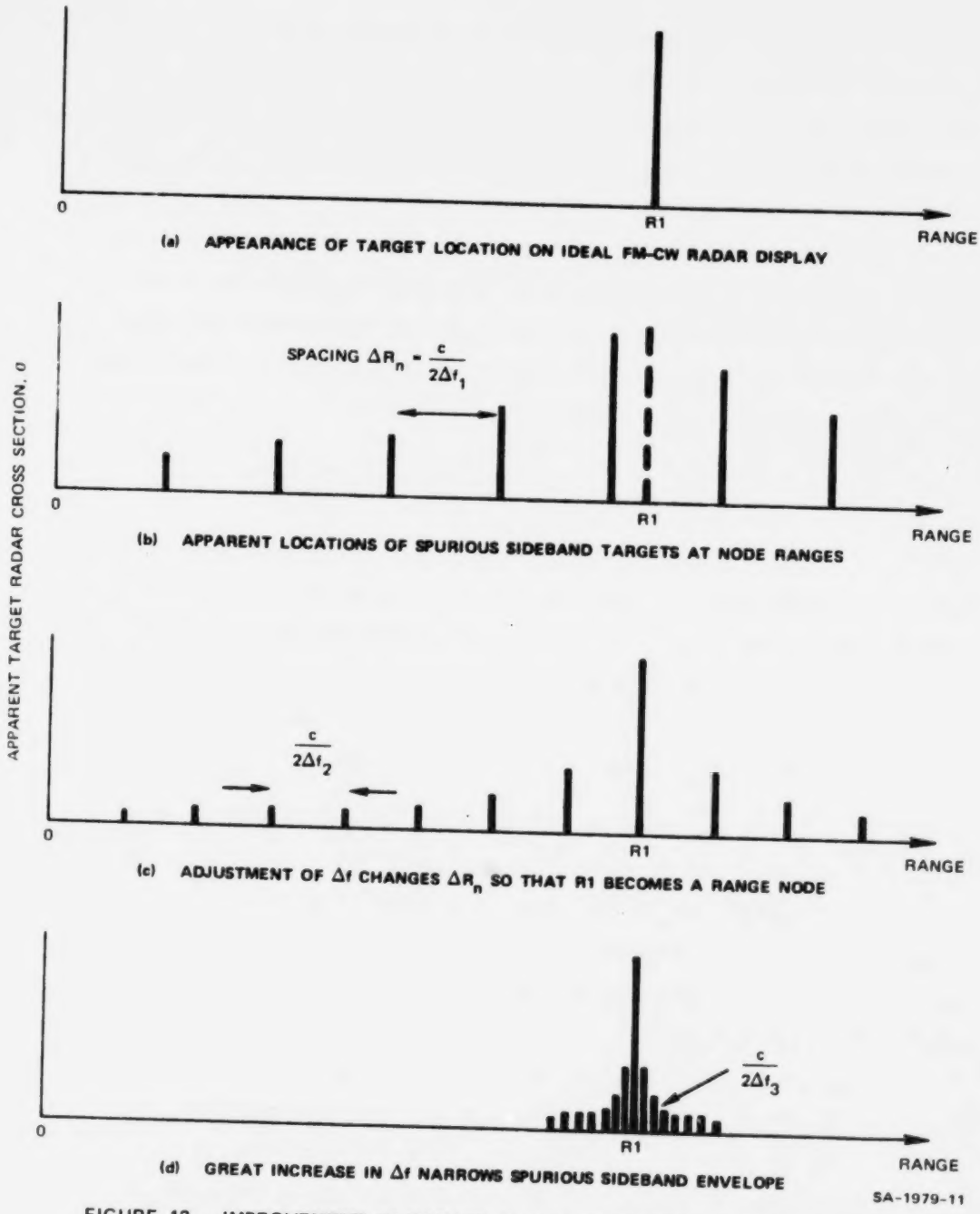

FIGURE 13 IMPROVEMENT IN TARGET RANGE RESOLUTION BY INCREASING DEVIATION, Δf

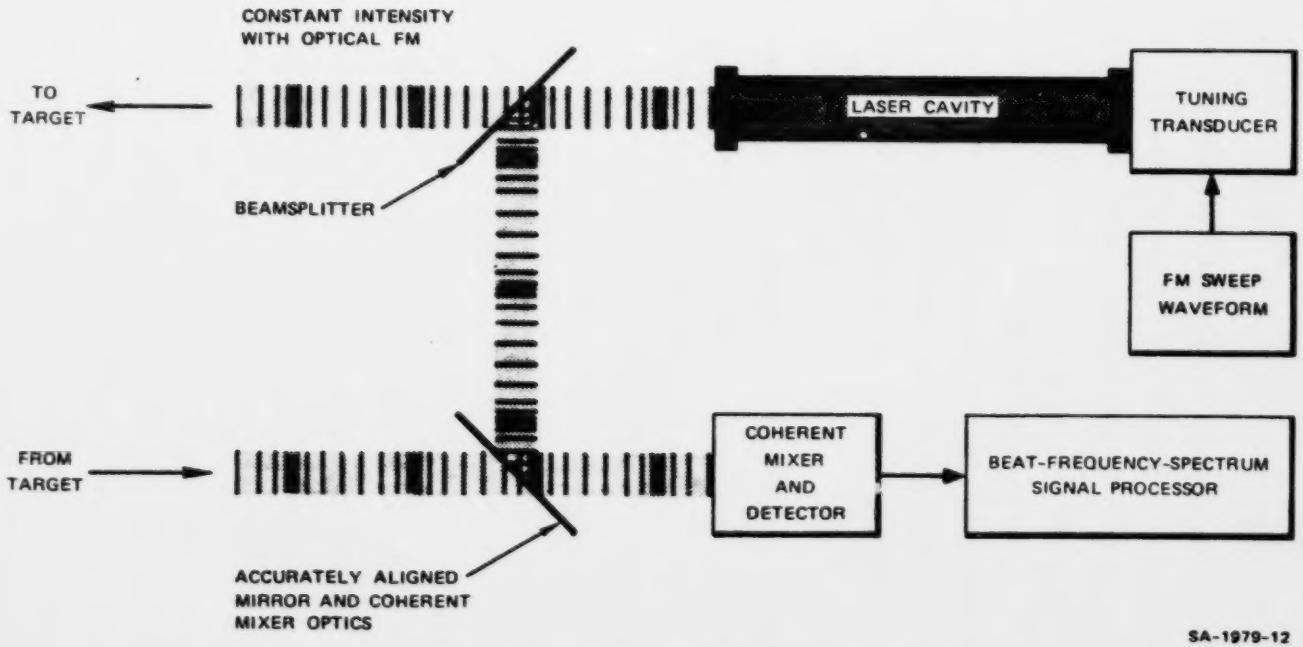

FIGURE 14 OPTICAL FM–CW RADAR MODULATION

Certainly the practicality of these lasers is questionable in a low-cost, field-portable lidar to be developed within three years.

Moreover, optical FM requires optical-frequency mixing in order to generate the beat-frequency spectrum showing the target range-vs.-power profile. Such coherent mixing requires very carefully aligned receiver optics and a photodetector capable of extracting a beat-frequency envelope that could have a microwave bandwidth in its own right. These requirements can all be met with advanced components and techniques available today, but few if any lend themselves well to the low-cost, durable, field-portable instrument design that is the primary goal in this effort.

Finally, since the optical-carrier and FM-signal wavelengths are on the order of target particle size and spacing, the coherent effects of multiple scattering and optical Doppler shifts could combine to put complicated and possibly deleterious noise components into the signal spectrum. The kind of holographic signal processing required to extract optical-frequency signals from such noise must come from a very new and still unexplored technology. The design problems posed by a coherent, optical FM system are very interesting, but their solution is significantly more difficult than an overall change in technique.

Given this perspective on optical FM, another modulation technique appears to be the more promising design approach. By using the optical carrier only to obtain high lidar target cross section, and employing much lower VHF or HF intensity modulation to obtain the range-profile information, the best of existing CW laser and HF electronics technology can be exploited. This hybrid technique, used successfully in ranging experiments during this study, might more properly be called FM-AM-CW radar modulation. Figure 15 shows a convenient way of envisioning this modulation technique. A carrier signal centered, for example, at

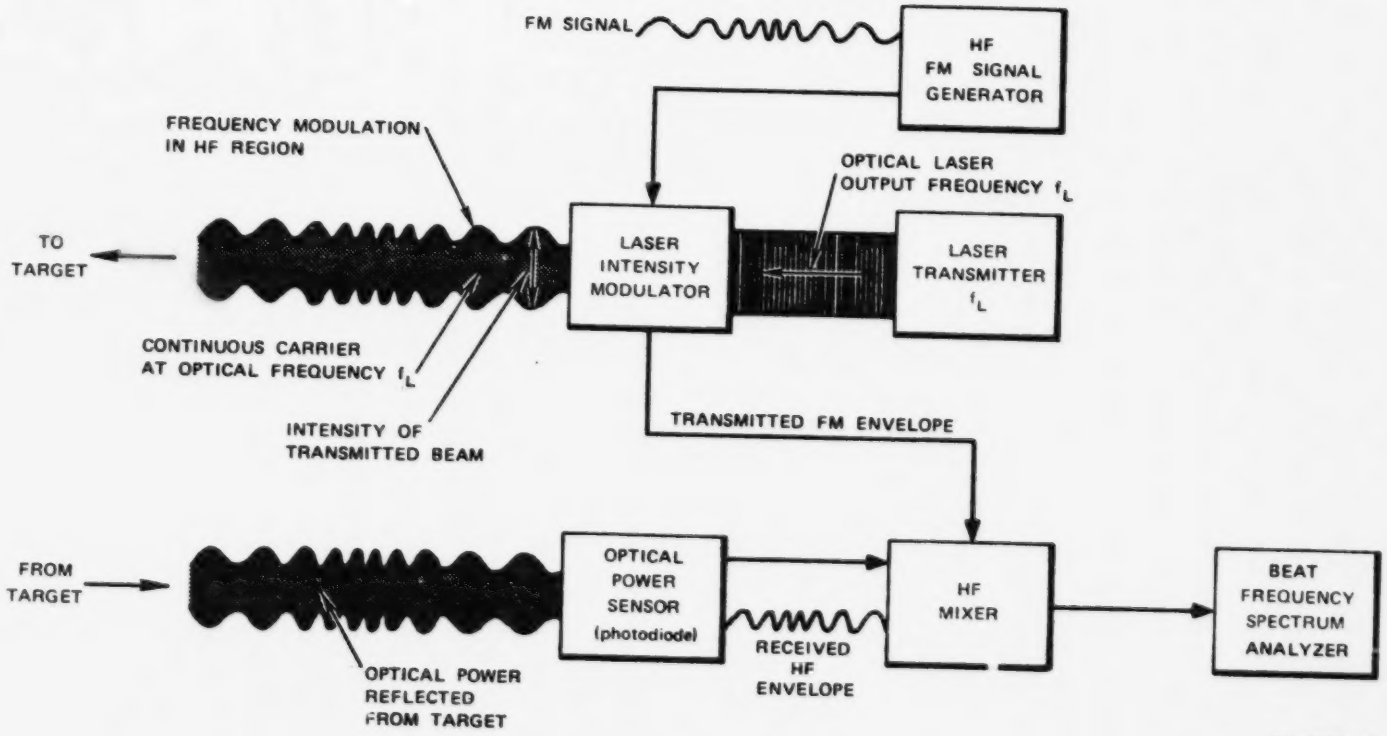

FIGURE 15 FM–AM–CW RADAR MODULATION

10 MHz, is frequency-modulated through a deviation Δf of 6 MHz--i.e., from 7 MHz to 13 MHz. This FM signal is then used to modulate the intensity (AM) of a laser-beam carrier operating continuously (CW) at one optical wavelength. As Figure 15 indicates, the FM signal envelope is detected by the photosensor and processed by electronics consisting only of low-cost, medium-frequency components. The radar system remains linear in the sense that a target whose optical cross section, σ, increases by a factor X will reflect an HF signal envelope that is also larger by X. When heterodyned with the transmitted FM signal, a target signal at beat frequency, f_R, will result that is also X times greater in amplitude than before. The equipment needed to implement the hybrid FM-AM-CW lidar modulation is readily available from well developed commercial technology.

c. Modulation Equipment

From examination of the block-diagram elements in the modulation scheme shown in Figure 15, it is apparent that the key element is the FM-signal generator used both to modulate the laser-beam intensity and to beat down the received signal in the mixer. The requisite sawtooth (or triangle) sweep can be generated as a voltage waveform by any of a wide variety of function generators. When this waveform is used to drive a voltage-controlled oscillator (VCO), the oscillator's output frequency will have the appropriate FM sweep waveform [Figure 16(a)]. Simple variations in voltage offset and sawtooth amplitude can be made as adjustments, causing corresponding variations in FM-sweep center frequency and total deviation, respectively. Likewise, errors such as drift or nonlinearity in the voltage-function generator will cause frequency shifts and nonlinear-sweep errors in the FM signal. Moreover, the VCO will have an input bandwidth that must be considered in designing the input-voltage function generator. A triangle wave at

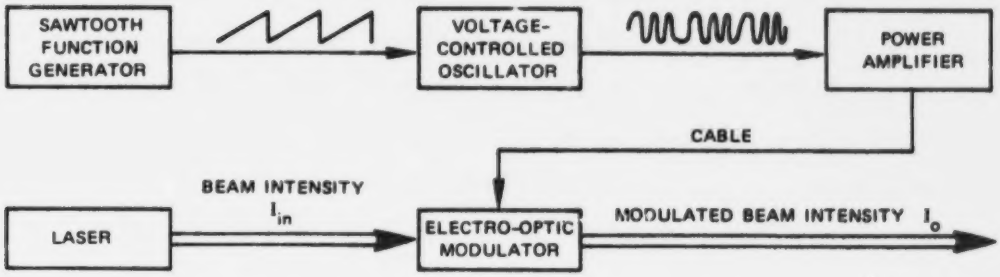

(a) A PRACTICAL CW LIDAR MODULATOR DESIGN

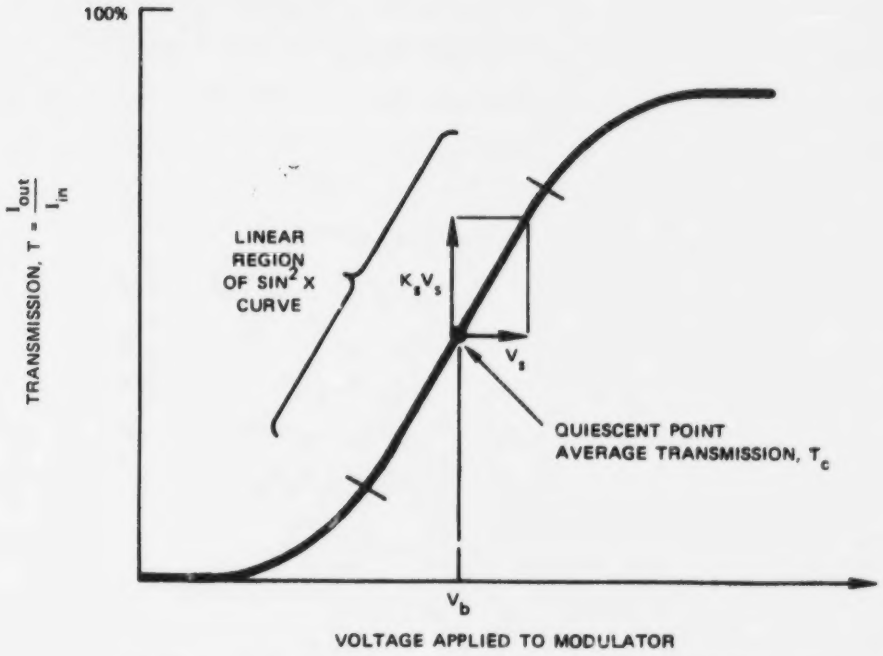

(b) ELECTRO-OPTICAL CRYSTAL MODULATOR TRANSMISSION CHARACTERISTIC

SA-1979-14

FIGURE 16 ELECTRO-OPTICAL MODULATOR PERFORMANCE

repetition frequency f_m will be accurately reproduced by a system whose bandwidth accommodates the triangle's primary Fourier components at f_m, $3f_m$, and $5f_m$. For example, a VCO with an input bandwidth of 100 kHz will not pass the third and fifth harmonics of a 50-kHz triangle wave, and its resulting FM sweep will resemble more a sinusoidal sweep at 50 kHz. As discussed earlier, a nonlinear sweep like this tends to add spurious sideband components to the target display of an FM-CW radar. Therefore, it is imperative that the sweep repetition rate fall well within the VCO input bandwidth.

Once a clean FM signal has been generated, it needs to be sent to both the laser-beam intensity modulator and the mixer. If the connecting cables do not have a flat response over the sweep frequency range, an additional AM component will be introduced on the FM signal. This FM-to-AM conversion can be a significant cause of spurious sidebands in the target-spectrum display. If buffer amplifiers or power amplifiers are used to interface the FM signal with other system components, the amplifier response must also be uniform over the sweep region Δf.

The next key modulation component to consider is the laser-beam intensity modulator. The most well developed, off-the-shelf component is a type of electrooptic crystal such as KDP whose optical transmission changes with increasing voltage applied to opposite faces of the crystal. The intensity, I, of the output changes with applied voltage, V_S, according to the following equation:

$$\frac{I_{out}}{I_{in}} = \sin^2\left[V_S + V_b\right] \quad . \tag{21}$$

A judicious choice of the bias-voltage value V_b and the range of the argument $[V_S + V_b]$ allows operation along the nearly linear portion of the $\sin^2 X$ curve, so that the useful modulator function becomes:

$$\frac{I_{out}}{I_{in}} = KV_S + T_C \qquad (22)$$

where K and T_C are constants related to the shape and center point of the optical transmission characteristic of the modulator assembly (see Figure 16).

The applied voltage changes the transmission of the modulator in a linear, analog fashion. KDP modulators typically offer excursions of 100:1 in transmission at bandwidths up to 10 MHz, and even up to 25 MHz with special driving circuitry. Once again, the nonlinearities introduced by the modulator's $\sin^2 X$ characteristic and bandwidth can degrade the FM signal appearing on the optical carrier in such a way as to introduce spurious sidebands in the final target display. The better the reproduction of the original sawtooth frequency sweep, the closer the lidar performance is to that modeled in Section IV-A. It should be clear from the present discussion that the design and specification of modulator components is very important in reducing system sideband noise. It is also important to note here that since the transmission of the modulator assembly is varied about an average value T_C, the average transmitted beam intensity is nonzero. The resulting dc component in a square-law-detected signal envelope has an important effect on system performance and must be carefully considered during the design of the lidar receiver.

2. Laser Transmitter

The incentive for using an optical radar wavelength lies in the nature of the intended target. Since a radar designer's goal is to maximize the amount of signal power to be detected after reflection or backscattering by the target, the designer should choose an operating wavelength smaller than the target dimensions. For particulate targets such as the aerosols and molecular constituents of the lower atmosphere,

relatively high backscattering and cross sections can be obtained for wavelengths less than 10 μm, at which a mix of Mie and Rayleigh scattering phenomena occur. As the radar wavelength shortens, the bulk-scattering cross section of the particles rises, but the corresponding path attenuation increases until in the far ultraviolet regions the useful lidar range may be too short to be practicable. On the other hand, in the infrared region the backscattering cross section is lower by an order of magnitude or more. A convenient middle ground is the visible region, particularly because presently acceptable techniques for judging smoke-plume opacity are visual. A visual technique is one involving the human eye, whose response to light peaks at green wavelengths. Because these visual methods typically involve comparison of plume darkness against the scattered blue light from the sky, a laser wavelength in the green is a reasonable choice for a CW lidar opacimeter that is to complement or even supplant existing remote-measurement techniques. Also important, most photodetectors are more efficient and sensitive to green light than to longer, red wavelengths.

Power output levels from 10 mW to 1 watt can be supplied by such commercially available CW gas lasers as the HeCd and argon types operating at various wavelengths between 4416 and 5145 Å. The stability, durability, ease of handling, and lower cost of HeCd and argon lasers also make them likely prospects for use in a mobile or field-portable instrument. CW tunable dye lasers have recently appeared on the market and may prove suitable in the present application should their prices drop significantly. They might also provide a means to identify the chemistry of the effluents. However, for basic plume transmission measurements at a single wavelength, a tunable CW laser would be more sophisticated than is required.

The power level actually required from the laser transmitter is constrained at the upper extreme by laser-performance and eye-safety

considerations and at the lower end by receiver sensitivity and background noise.

HeCd lasers are now available that can transmit up to 50 mW at 4416 Å. Argon lasers with rated power outputs from 25 mW to 10 watts can transmit at any of a number of wavelengths: 5145, 4880, 4765, and 4579 Å. The trend toward standardizing transmissometer sources to the green region favors use of the argon 5145-Å line. Such factors as tube life, cooling requirements, line stability, and electrical power drain can limit the choice of such an argon laser to one of the lower power models for mobile or field-portable applications. Also, the ability of the electrooptical modulator crystal to handle the rejected beam power during its attenuating half-cycles limits the amount of power that can be transmitted by an FM-CW lidar.

Finally, eye-safety considerations indicate that the transmitted beam intensity should not exceed approximately 1 mW/cm^2. This number is derived from data showing the interrelations between continuous source radiance, retinal irradiance, retinal image size, and thermal damage (if any) done before the eye's natural blink reaction occurs.[12] For example, if the lidar receiver design shows that one watt of power must be transmitted to a target in order to get a detectable return signal, the transmitted beam's cross-sectional area should be 10^3 cm^2 or greater. This in turn means that the transmit lens must be some 40 cm in diameter in order for the one-watt beam to be eye-safe even for personnel looking directly into the transmit aperture. Given the receiver's sensitivity and the target's lidar volume backscatter cross section, eye-safety considerations then lead to the first step in the design of the transmitter optics: choosing the output-aperture dimension. The remainder of the transmitter's optical design is straightforward and, since it has no peculiar dependence on the CW technique, will not be pursued here.

Internal laser noise is one additional characteristic that can have a serious effect on CW lidar performance. Since the CW lidar target information is contained in the frequency spectrum, the spectral characteristics of noise become important. Appearing as either spectral base line "grass" or as spectral line-broadening frequency instability, the noise components can interfere with the desired target signal spectrum.

Laser amplitude noise can be caused by the 60-Hz harmonics riding on top of the dc gas ionization or exciter voltage. Amplitude noise can also appear in the VHF region of the spectrum at a beat frequency between two laser modes. Since both of these AM noise sources steal carrier power and introduce it as spurious sideband components, the designer must either specify components that reduce the noise level or choose modulation parameters so that the spurious noise components will not fall in the target signal spectrum, or both.

In a similar fashion laser frequency instability can cause a kind of FM noise that is converted into AM noise in the laser itself. The severity of this internal FM-to-AM noise conversion is difficult to estimate and even more difficult to measure in the presence of other FM-CW system noise sources. Laser manufacturers claim that laser FM noise is generated by acoustical disturbances to the laser cavity caused by the flow of cooling air or water, loud noises, or random motions of the laser mount. Since all these phenomena occur in the audiofrequency range, such internal noise could show up as low-level audiofrequency components on the detected high-frequency modulation envelope. On the other hand, atmospheric effects can also convert the VHF frequency instabilities directly into VHF AM noise, as discussed later.

3. Optical Receiver

The design of an optical receiver for incoherent, square-law detection of backscattered laser signals has been amply discussed by others.[2,13] A few receiver characteristics, however, have effects on performance that are peculiar to an FM-AM CW lidar and should be examined here.

The modulated laser-beam intensity was expressed in Eq. (22) as

$$I_o = I_{in}\left[KV_S + T_C\right] \quad . \tag{22a}$$

Since $V_S = V_o \sin[2\pi f_o t]$, where f_o is the FM sweep function, the average value of $I_{in}KV_S$ is zero. However, the quiescent modulator transmission value T_C is nonzero, and therefore an average nonzero intensity equal to $I_{in}T_C$ is continuously transmitted. Since the laser modulator input intensity I_{in} is very nearly constant, consider I_o instead as

$$I_o = K_S V_S + K_C T_C \quad . \tag{23}$$

The amount of transmitted power reflected from a target at range R is proportional to I_o, and the amount of power scattered into the receiver is also proportional to I_o. Including target cross section, path attenuation, R^2 losses, and the receiver aperture A_R as a constant of proportionality, K_1, the received power P_R can be expressed as

$$P_R = K_1 I_o$$

$$P_R = K_1 K_S V_S + K_1 K_C T_C$$

which can be redefined as two power components

$$P_R = P_S + P_C \quad . \tag{24}$$

The most sensitive, low-cost light detectors for use in this application are square-law detectors such as a photodiode or photomultiplier tube (PMT). The current output of the detector is proportional to incident power, so that in the case above, output current is:

$$i_R = i_S + i_C \tag{25}$$

where i_S is the FM sinusoidal function and i_C is a constant. The relative value of i_C/i_S is just the ratio of modulator parameters $K_C T_C / K_S V_S$. This value typically averages 1.5 and higher for practical electrooptic-crystal laser-beam modulators. As a rule, the better the modulator's reproduction of the input signal, the higher the value of $K_C T_C / K_S V_S$. The resulting effect is that the average dc component, i_C, could exceed the continuous current rating of the detector for a bright lidar target. Another result for a slightly smaller target return would be that i_C could drive the detector nearly into saturation, thereby reducing the effective gain for the smaller, information-bearing current, i_S.

Even when both i_S and i_C are in the dynamic range of the detector, i_C creates a steady, additional shot-noise component above that of i_S. In short, the relatively larger reflected power component P_C contains no information, yet it can significantly reduce the lidar system's signal-to-noise ratio (SNR) in the case of a strong target echo. The dc component can mask the returning, information-bearing FM sinusoidal signal, P_S. The design of the lidar receiver should therefore take into account both the modulator parameters $K_C T_C$ and $K_S V_S$ and the maximum expected target reflectivity. As a practical matter, since the lidar

operates continuously, it lends itself well to incorporation of an automatic gain control (AGC) to reduce PMT gain for bright-target conditions. An AGC could keep both i_S and i_C in a range where i_S can be separated, undistorted, from i_C in signal-processing circuits.

Considering the distributed nature of the atmospheric target particles, an experienced lidar designer would point out here that certainly the backscattered signal from ranges very close to the receiver would be decades stronger than those from distant targets, and would therefore mask remote-target information whether there is an AGC or not. The solution for a pulsed lidar is, of course, to make sure that the receiver's field of view does not intersect the transmitted beam for some appropriate distance from the receiver. This is not a complete solution for a CW lidar, however. The continuous average signal effects discussed in the foregoing paragraphs combine in the receiver's field of view to introduce a spatial integration effect on the CW lidar's distributed-target performance at any range.

The modulated laser beam, frozen in an instant of time, would appear as a column of light with alternating light and dark sections spaced at the modulation wavelengths (Figure 17). For a constant modulation frequency f_o, the peaks are spaced by $\lambda_o = c/f_o$. A receiver viewing one thin slice of one section will see the full maximum and minimum value of the intensity as the column is allowed to proceed across the field of view at the speed of light. As the field of view is increased to include one-half wavelength, the receiver will capture greater total power, but the relative ratio of the total's maximum to its minimum will fall because, just as a dark region is leaving the field of view, a light region is entering. When the receiver views a full wavelength, again the total average received power increases, but the minimum value of intensity for the dark section is exactly offset by the maximum values being received from the light section at any instant of time.

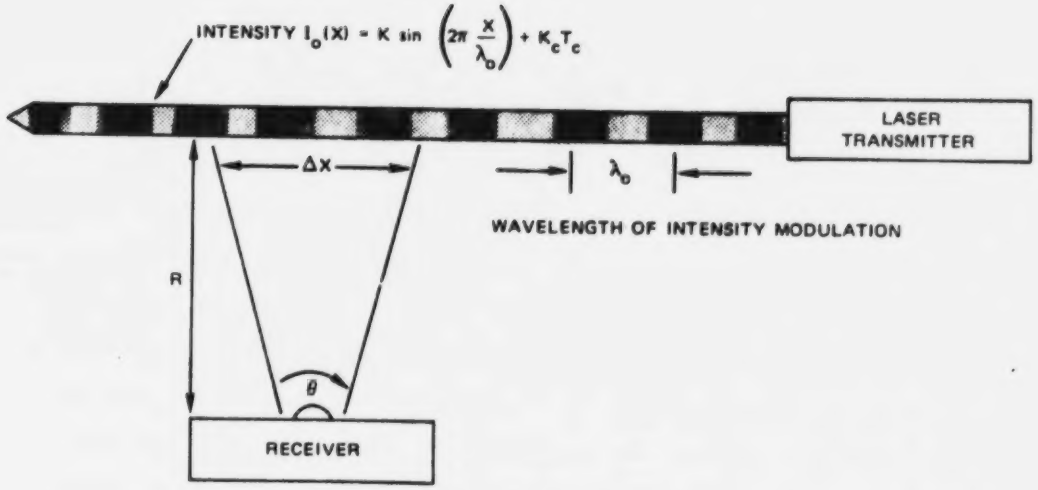

(a) SIMPLIFIED ANALYTICAL MODEL

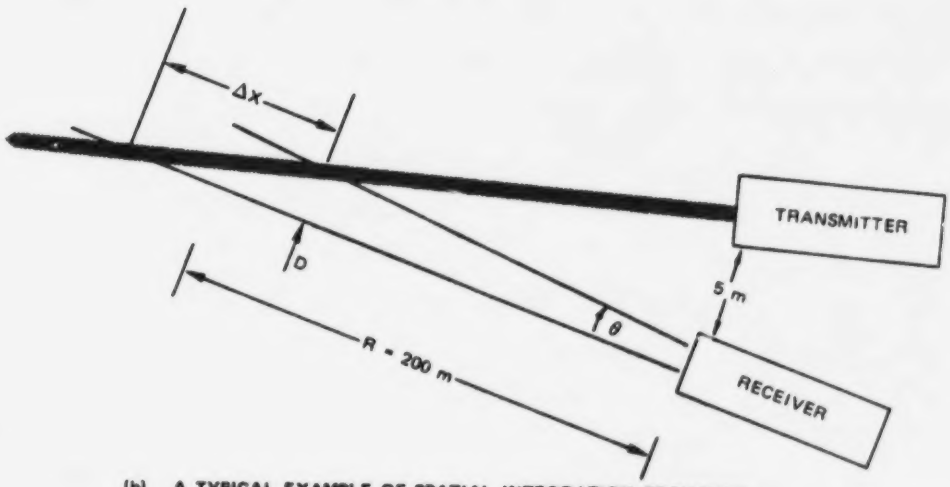

(b) A TYPICAL EXAMPLE OF SPATIAL INTEGRATION GEOMETRY

SA-1979-15

FIGURE 17 SPATIAL INTEGRATION OF BEAM INTENSITY FUNCTION BY RECEIVER

In the expression for intensity of the frozen column of light as a function of length, it is clear that every time length x increases by one wavelength λ_o, one cycle is completed:

$$I_o(x) = K_S V_O \sin\left(2\pi \frac{x}{\lambda_o}\right) + K_C T_C \quad . \tag{26}$$

Of course, when the beam is allowed to move again, the length x traversed by a modulation peak at the speed of light is just x = ct, which, when substituted in the sine argument above, gives Eq. (23) for $I_o(t)$.

The lidar receiver field of view, θ, encompasses at any instant some extent of beam length Δx where $\Delta x = \theta R$ at range R. The power received is just the integral of the intensity function over the spatial extent Δx that is being viewed:

$$P_R = K_1 \int_x^{x+\Delta x} K_S V_O \sin\left(2\pi \frac{x}{\lambda_o}\right) dx + K_C T_C \, dx \tag{27}$$

$$P_R = K_1 K_S V_O \frac{\lambda_o}{2\pi} \left[\cos\left(\frac{2\pi}{\lambda_o} x\right) - \cos\left(\frac{2\pi}{\lambda_o} x + \Delta x\right)\right] + K_1 K_C T_C \, \Delta x \quad . \tag{28}$$

The power received at an instant of time is clearly a function of field of view, because Δx is the extent of the beam subtended by the field of view at range R. Also, since the value of x is arbitrary, depending on where the beam is frozen in space and phase, Eq. (28) can be simplified by letting $x = \lambda_o/4$ so that:

$$P_R = K_1 K_S V_O \frac{\lambda_o}{2\pi} \cos\left(\frac{2\pi}{\lambda_o} \Delta x\right) + K_1 K_C T_C \, \Delta x \quad . \tag{29}$$

As the field of view is widened, the term $K_1 K_C T_C \, \Delta x$ increases linearly. However, the cosine term periodically peaks at $K_1 K_S V_O \, \lambda_o/2\pi$ every time Δx reaches an integral multiple of wavelength λ_o. The peak value of the

information-bearing cosine signal can be expressed as a fraction P_{rel} of the nonzero average power:

$$P_{rel} = \frac{K_1 K_S V_O \frac{\lambda_o}{2\pi}}{K_1 K_C T_C (\theta R)} = i_{rel} = \frac{i_s}{i_c} \quad . \tag{30}$$

It is clear that as receiver field of view increases, the detected sinusoidal signal current drops in relation to the average dc current. Since the average dc component is a noise source and a limiting factor as discussed earlier, an increasing field of view acts to degrade system SNR independent of optical background noise.

Therefore, in a CW lidar system, the receiver ideally must view less than one-half wavelength of the modulating frequency f_o. As the field of view widens, the stronger dc-induced noise swallows up the frequency component f_o.

Similarly, when f_o is a sweep function of time, $f_o(t)$, in order for the receiver's response to a distributed target to be uniform for each frequency in the sweep range Δf, the receiver must view at most a fraction of the wavelength of the highest modulating sweep frequency, $f_{o,max}$.

As an example, assume that the maximum sweep frequency is 10 MHz, so that $\Delta x < 15$ m is the spatial integration constraint. Assume also that the target is at 200 m, and that the receiver can be no further than 5 m from the transmitter [Figure 17(b)]. If the receiver is to view only Δx, its beam diameter at the target must be

$$D \approx \left(\frac{5}{200}\right)(15 \text{ m}) = 0.4 \text{ m}$$

and therefore field of view θ should be smaller than

$$\theta = \frac{D}{R} = \frac{0.4}{200} = 2 \text{ mrad}$$

which is not an unreasonable practical constraint.

4. Atmospheric Effects

Just as pulsed-lidar performance is affected by atmospheric turbulence and nonuniform aerosol or particulate concentration, the CW lidar beam undergoes these atmospheric effects. Unlike the pulsed system, however, the CW lidar continuously reads out the magnitude of error introduced by these effects. For example, if, in the idealized lidar of Section IV-B, the backscattering coefficient of the near clear-air volume changes while that of the far volume does not, the continuous readout of $[\log P_{near} - \log P_{far}]$ would vary accordingly about an average value. A chart recording of this relative reading would show the magnitude of excursions from the average value, giving a quick and reliable measure of system accuracy under changing atmospheric conditions. An operator would know in a minute or two whether conditions were too turbulent for adequate plume-opacity measurements. Indeed, microwave FM-CW radar has been used recently specifically to measure air turbulence.[14,15]

Additional atmospheric phenomena may have deleterious effects on the beam's modulation envelope. In this experimental study, noise from these peculiar effects did not appear significantly above other system noise levels. Nevertheless the design of an FM-CW lidar should take them into consideration.

Particles and molecular constituents of the atmosphere are not at all stationary when they scatter light. For example, molecular oxygen at 273° K consists primarily of molecules moving at speeds between 10^4 and 10^5 cm/s. Recall that a moving target or scatterer shifts the frequency of any signal that it reflects along its velocity vector. For a

radar signal frequency f_o, velocity v, and speed of light c, the Doppler-shift frequency f_D is:

$$f_D = \frac{v}{c} f_o \quad .$$

For a laser beam at $f_o = 6 \times 10^{14}$ Hz, where f_o is the optical carrier frequency, oncoming oxygen molecules could shift the received signal frequency by as much as 2 GHz. Since the various scatterers in a volume of clear air are moving with a continuum of velocity components along the lidar-beam axis, the Doppler shift in the color of the reflected laser light would be a continuous spectrum from 0 to 2 GHz around the optical carrier frequency. In an optical FM-CW radar such as that shown in Figure 14, the random Doppler shift in the optical FM sweep signal would be on the order of the sweep deviation Δf obtainable from the tunable laser. Therefore a change in return-signal frequency (color) due to Doppler shift would be similar in magnitude to the intended frequency changes due to target-echo delay time. As a result, Doppler effects from the distributed atmospheric scattering target could cause serious inaccuracies in the target range profile in a coherent, optical heterodyne system.

In an FM-AM-CW lidar, however, the range information is contained not in optical FM but in the VHF or HF modulation envelope around the optical carrier's intensity (Figure 15). The photodiode receiver throws away the optical-carrier frequency information; changes of 20 GHz in a 6×10^{14} Hz laser frequency would not be detected in such a receiver. Only the HF envelope signal is processed. Its highest frequency during the sweep is on the order of 10 MHz, and it too undergoes a Doppler shift due to atmospheric particle velocity:

$$f_D = \frac{10^3}{3 \times 10^8} \times 10^7 = 33 \text{ Hz} \quad .$$

This shift is small compared to the value of $\Delta f = 5$ MHz used in a practical FM-AM-CW lidar, and is also small compared to the resultant beat frequencies, typically 100 kHz or so for a target range of 200 m.

A second atmospheric effect, coupled with Doppler shift, could conceivably add amplitude noise to the Doppler-frequency noise just discussed. The severity of this new effect is difficult to calculate; measuring it was one of the main goals in this recent effort. It is another manifestation of the FM-to-AM noise conversion mentioned earlier. The theory behind this second effect is cumbersome to express mathematically. A qualitative explanation will help here.

Those who have observed an object illuminated by a laser have undoubtedly noticed a kind of speckle pattern overlaid on the object. The pattern is caused by constructive and destructive interference of wavefronts emanating from various point reflectors on the object. Whether a particular point will appear to be a bright or dark speckle is determined for a given beam diameter by (1) spacing between points on the object, (2) distance to the observer's eye, (3) observer's pupil size, and (4) the wavelength of the laser light. When the observer moves his head he sees the speckle pattern change, as if the object were glistening. He is changing the angle between lines drawn from two given object points to his eye. As the two path lengths change, the apparent source brightness goes through bright and dark interference cycles. In effect, changing the determinants of the speckle pattern causes intensity variations, or "AM noise" at the observer's eye.

In a similar fashion, a stationary lidar receiver viewing moving point scatterers will see a glistening image. Its intensity appears to vary as any two scatterers move into the field of view in such a way as to cause interference fringes to move across the receiver aperture.[16] As the aperture is enlarged, the effect decreases because more

fringes are being spatially integrated over the aperture dimension, and any new fringe moving in amounts to a smaller percentage of the whole pattern. Similarly, two scatterers in the field of view may have Doppler-shifting wavelengths as well as shifting positions that can cause speckle variations. The glistening speckle effect caused by billions of individual scatterers at various speeds, ranges, and angles-off-axis might be complicated and serious enough to cause significant AM noise in the received signal. Theoretical analysis of this point becomes quite difficult, and in the absence of experimental data one could speculate that the AM noise might be dominated by the optical Doppler shifts, which would add noise with bandwidth up to 2 GHz on the return signal. Or the AM noise might be caused only over relatively small spatial regions, so that only a very small receiver aperture or narrow field of view would be adversely affected. The effect might be serious for an optical FM-CW lidar with its need for coherent heterodyning, while not showing up at all in an FM-AM-CW system.

As a practical matter, during this experimental study, no serious Doppler or FM-to-AM conversion noise occurred to degrade system performance. If any of these noise phenomena occurred, their contribution was below that of other readily identified and correctable system sources. It is not certain, however, that an optical design for an FM-AM-CW system somewhat different from the one used here would also be free of this noise. Nor is it clear that a purely optical FM-CW coherent radar would escape these effects. Future CW lidar designs should not ignore the potential for such Doppler spreading and FM-to-AM noise conversion to degrade system performance. However, actual results show that at least one FM-AM-CW lidar design is largely free of these adverse atmospheric effects.

5. Signal Processing

The foregoing sections have discussed the design of an FM-AM-CW lidar without specifying the manner in which the received signal frequency is subtracted from the transmitted signal, nor the method for displaying and measuring target range and returned signal power. Some theoretical considerations of measurement uncertainty were discussed in Section IV-C-1-a, but an explanation of the signal-processing functions required in an FM radar still needs to be presented.

In Section IV-C-1 the advantages of VHF or HF frequency mixing as opposed to optical, coherent heterodyning were pointed out. Indeed, in the FM-AM-CW technique any of a number of inexpensive, commercially available HF mixers can be used. Such mixers contain nonlinear elements that multiply the transmitted FM signal envelope with the delayed, received envelope to generate sinusoidal signals at the sum and difference of the input frequencies. Since only the difference component is of interest the mixer must be followed by a low-pass filter that eliminates the higher sum-frequency components.

Practical mixers have limits to the dynamic range over which their conversion of input-signal to output-signal amplitude is linear. Care must be taken to guarantee that the photodetector output does not exceed the mixer's maximum linear input level. Otherwise, comparisons of various frequency-component amplitudes will be inaccurate. The mixer will also introduce internal conversion noise around the signal during the heterodyning process. If the input signal is small enough, mixer noise can overwhelm it. There is also a conversion loss through the mixer that typically attenuates the signal power by a factor of five or ten. While mixers are functionally simple to use, their detailed input-output characteristics can be quite important in the design of a CW lidar, where low-level and wide-dynamic-range signals are expected.

Once the mixer output has been obtained and sum-frequency components filtered out, it remains to analyze the spectrum of the difference-frequency signal and noise. As discussed in the foregoing sections, this spectrum contains the target range and reflected-power information that is of primary interest to the operator. Signal processing at this point is required to perform the following functions:

(1) Determine the frequencies of interest.

(2) Extract the target signal spectrum from the noise spectrum.

(3) Modify and format those signals in such a way as to provide a convenient measurement of target characteristics.

Function 1 is simple when the system's modulation parameters and target characteristics are known. A narrow bandpass filter tuned to the known target frequency will eliminate all components except the target-frequency component. If there are three targets, three such narrow-band filters can be used, as in the idealized CW lidar opacimeter discussed in Section IV-B. A portable AM radio does much the same thing: it can be tuned to a predetermined broadcast frequency to process the voice or music signals found there.

When the target spectrum is not known in advance, as in this research and development effort, it is necessary to scan through the frequency spectrum until an overall picture of the target range has been developed in order to find any interesting spectral characteristics. A spectrum analyzer is a useful instrument for this purpose. It sweeps a narrow-band filter of some bandwidth B from zero frequency to some maximum frequency, displaying component amplitude Y versus sweep position X. While it is certainly beyond the scope of this report to explain spectrum analyzer theory, it can be said that the instrument is of great utility as a development tool. But since it cannot view three separate

frequencies simultaneously, one cannot always use the analyzer to make instantaneous comparisons of the reflected power levels of FM-CW lidar targets. The analyzer takes some time to sweep from the frequency of the near target to that of the far target. During that sweep time, the target characteristics may have changed, and therefore the analyzer sweep rate introduces uncertainties in measurements referenced to time-varying signals. For slowly changing signals, however, the scan rate may be fast enough to reduce the uncertainty to an acceptable level.

Functions 2 and 3 are straightforward electronic design problems and are not peculiar to the FM-AM-CW lidar technique. The idealized CW lidar for measuring smoke-plume opacity shown in Figure 7 includes functional signal-processing blocks that are readily achieved with inexpensive commercial components. In the CW lidar design the need for complicated signal processing can be reduced by careful design elsewhere in the system. A good choice of modulation and frequency parameters would allow the target spectrum components to fall away from, or in between, noise-spectrum components. For example, the so-called semiconductor 1/f noise spectrum diminishes in strength at frequencies above 10 kHz, while the modulator's power-amplifier signals may leak into the processor circuits as noise in the frequency range above 1 MHz. By choosing modulation rate f_m and deviation Δf carefully, the designer can cause the desired beat-frequency spectrum for targets between 100 and 300 m to lie between 30 and 500 kHz, thereby avoiding the given 1/f and leakage-noise spectra.

V EXPERIMENTAL PROGRAM

The objective of the experimental program undertaken here was to determine the engineering requirements necessary to design, fabricate, and operate a CW lidar with range and amplitude resolution sufficient to obtain transmittance measurements on semitransparent targets at ranges of 500 to 1500 feet.

After surveying some of the analytical groundwork described in the foregoing sections, the intensity-modulation, or FM-AM-CW, approach was selected over the less easily implemented coherent optical FM-CW technique. The next task included the design and construction of a laboratory-model CW lidar with flexibility for doing research over a wide range of parameters. With the completion of the lidar, preliminary system-noise and performance-limitation measurements were made. These measurements allowed the specification of optimum operating regions, and in these regions the first ranging and remote opacity measurements were made using the FM-AM-CW lidar. The details of these experimental program activities and their results are included in the following pages.

A. Design and Construction of a Laboratory-Model CW Lidar

The FM-AM-CW lidar technique chosen is depicted in Figure 15, and the modulator technique is detailed in Figure 16. For convenient reference this system has been redrawn in Figure 18, where each component is specified by function, manufacturer, and model number.

Item 1, the sweep function generator, is needed to provide very linear voltage ramps because the required linear frequency sweep $f_o(t)$, is patterned after this voltage waveform by the voltage-controlled

Preceding page blank

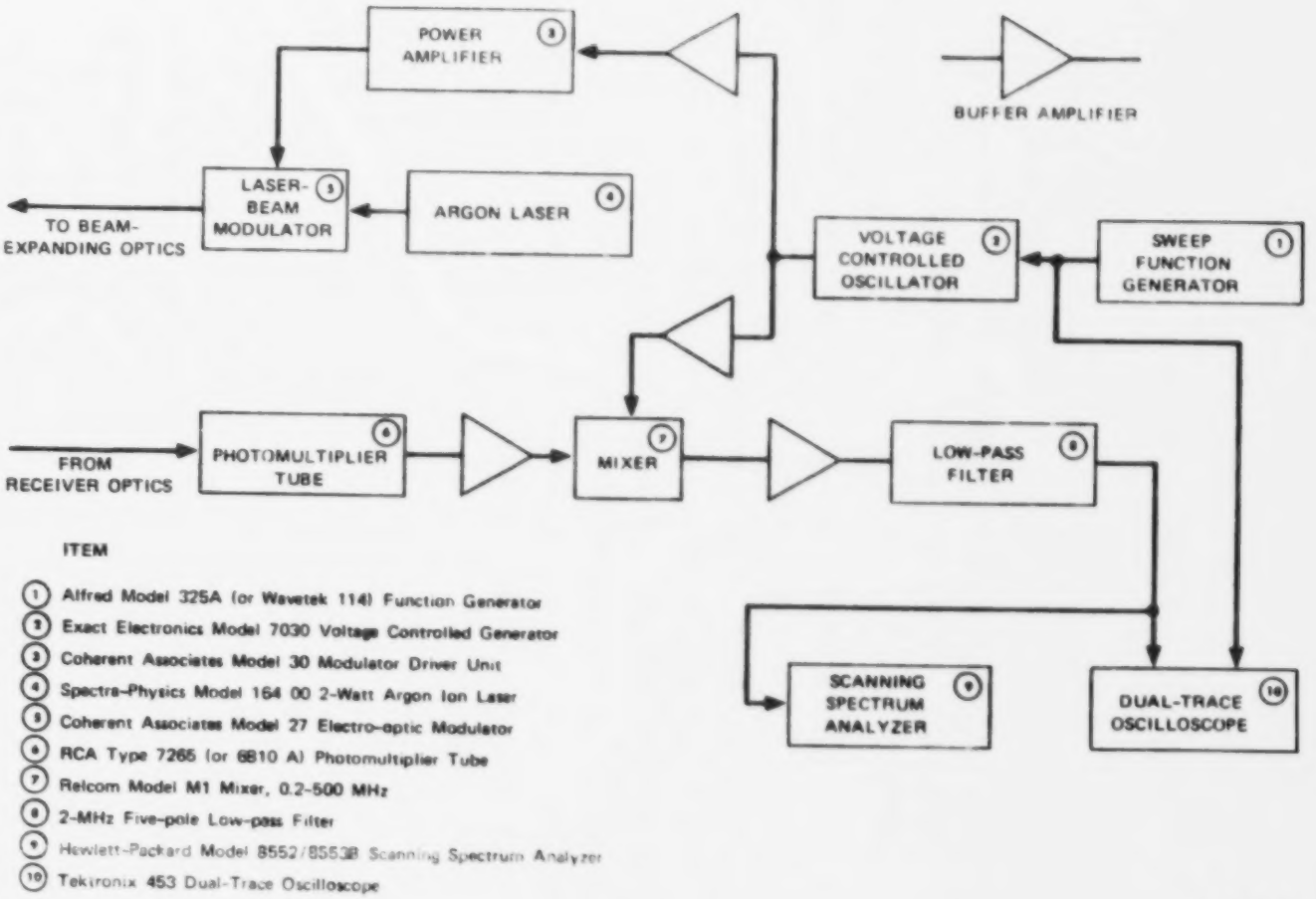

ITEM

1. Alfred Model 325A (or Wavetek 114) Function Generator
2. Exact Electronics Model 7030 Voltage Controlled Generator
3. Coherent Associates Model 30 Modulator Driver Unit
4. Spectra-Physics Model 164 00 2-Watt Argon Ion Laser
5. Coherent Associates Model 27 Electro-optic Modulator
6. RCA Type 7265 (or 8B10 A) Photomultiplier Tube
7. Relcom Model M1 Mixer, 0.2-500 MHz
8. 2-MHz Five-pole Low-pass Filter
9. Hewlett-Packard Model 8552/8553B Scanning Spectrum Analyzer
10. Tekironix 453 Dual-Trace Oscilloscope

SA-1979-16

FIGURE 18 LABORATORY MODEL FM-AM-CW LIDAR EQUIPMENT BLOCK DIAGRAM

oscillator, Item 2. The specified VCO had a remarkably linear voltage-to-frequency transfer characteristic. Its primary limitation was its input bandwidth, which tended to round off the sharp turnaround points on a triangular or sawtooth sweep waveform. This input bandwidth of 200 kHz limited the sweep repetition rate to $f_m < 20$ kHz in order to maintain sweep linearity and small relative turnaround time t_t. The majority of measurements were made using a 10-kHz modulation rate. Buffer amplifiers were used to reduce the load at the VCO output and thereby preserve signal purity.

The electrooptical modulator crystal (Item 5) has the measured voltage-to-transmission curve shown in Figure 19. The crystal presents a 65-pF capacitive load, requiring a rather powerful driver stage to provide the ±50-volt excursion around a bias point at 75 volts that makes maximum use of the linear portion of the modulator transfer curve. The

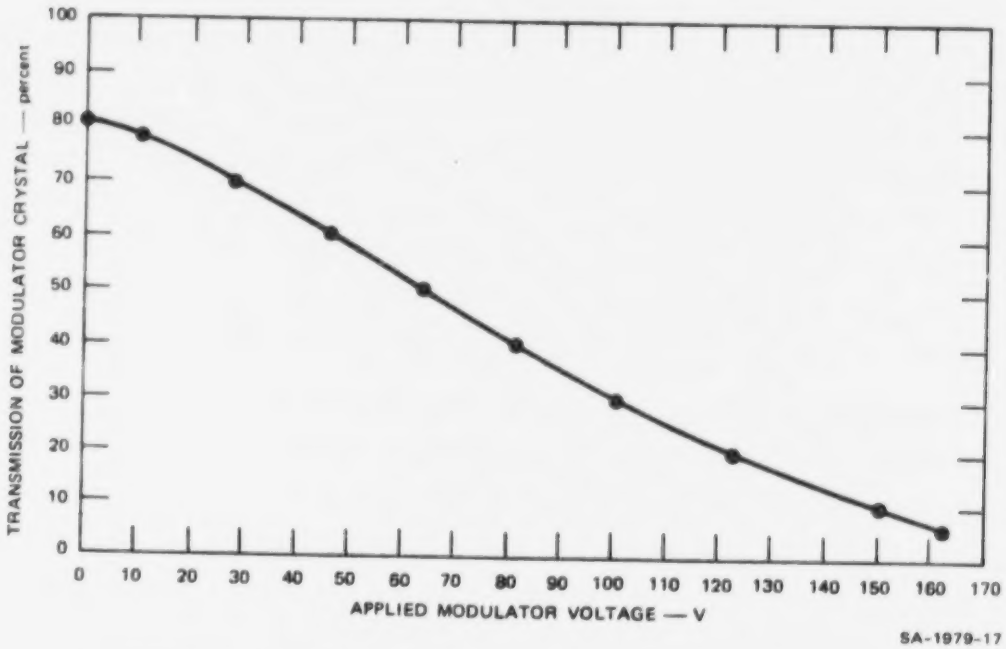

FIGURE 19 MEASURED MODULATOR TRANSMISSION CHARACTERISTIC

specified power amplifier, Item 3, is designed to drive the crystal at frequencies between dc and 10 MHz, a convenient range since the maximum frequency available from the VCO is 11 MHz. Moreover, spatial-integration effects in the receiver field of view dictated that the half-wavelength of the highest intensity-modulation frequency be no shorter than approximately 30 m to encompass reasonable smoke-plume targets. This factor also supports the choice of 10 MHz as an upper limit to the modulating frequency.

To achieve research flexibility, a durable, tunable, 2-watt Argon ion laser transmitter was specified (Item 4). The unit provided plenty of power for most experiments at 5145 Å. No internal laser noise could be measured save for 60- and 180-Hz ripple variations in the laser output intensity. These variations were well below the 60-Hz noise introduced by other components in the system such as the photomultiplier-tube power supply (Item 6). Only by purposely detuning the laser could one generate a beat frequency between two laser modes, but even then these beat frequencies were greater than 25 MHz, well out of the range of the overall 10-MHz system bandwidth.

The photomultiplier tube (Item 6) originally chosen for use as the laser receiver had an S-11 photocathode that introduced too much dark-current noise for adequate measurement of low-level backscatter from clear air. After switching to an S-20 phototube, it was possible to detect light backscattered from clear-air volumes at 100-m ranges.

Photomultiplier output current signals were buffered and mixed with the FM sweep drive signal supplied by the VCO. The output frequencies of the mixer consist of the sum and difference of the two input-signal frequencies. Since only the difference frequency is desired, a low-pass filter (Item 8) was used to eliminate the higher sum frequencies and pass

the lower beat-frequencies containing target-range information on to the display devices (Items 9 and 10).

Figure 20(a) shows the two kinds of data display employed in the operation of the CW lidar. The dual-trace oscilloscope display shows the voltage waveform (bottom trace) that drives the VCO; therefore this trace is an indicator of the FM sweep waveform, deviation Δf, and repetition rate f_m. The top trace is the output of the mixer showing the Fourier sum of all target-frequency components as well as the error-frequency components arising during sweep nonlinearities (note the blur in the trace corresponding to the turnaround points of the triangular sweep waveform). The second photo in Figure 20(b) is the spectrum-analyzer display (Item 9) of the frequency components comprising the top trace of Figure 20(a). Three main target frequencies appear, each of which is 10 dB above its surrounding sidebands. Indeed, when these photos were taken the lidar was viewing three targets downrange, and Δf had been adjusted to reduce each target's sideband envelope so that the three targets could be resolved on a display of the beat-frequency spectrum. Notice that the differences in signal power returned by various targets show up as height variations from component to component. By measuring Δf, f_m, and f_R from these displays, one can calculate target range from Eq. (7). By measurement of the heights of frequency components on the spectrum display, the relative power scattered back from the target ranges can be determined directly.

B. Target Display Characteristics

The goal of the overall effort is to develop a CW lidar for the remote measurement of smoke-plume opacity. The measurement of the distance to the plume is only incidental to this goal. Nevertheless, since analysis of FM radar performance shows that single, discrete targets will

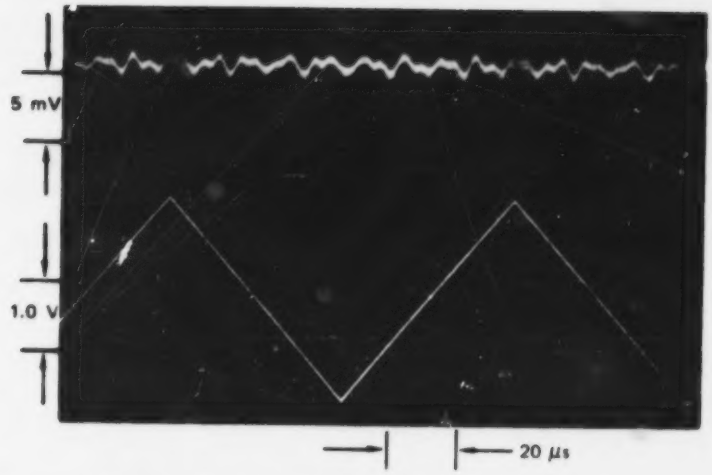

(a) OSCILLOSCOPE TRACE SHOWING MIXER OUTPUT SIGNAL (top) AND VOLTAGE WAVEFORM THAT DRIVES THE FM GENERATOR.

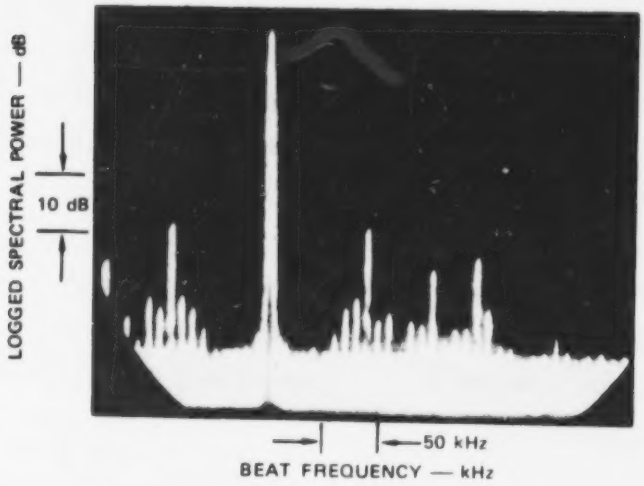

(b) SPECTRUM ANALYZER DISPLAY SHOWING THREE MAIN TARGET FREQUENCIES COMPRISING TOPMOST SIGNAL TRACE ABOVE. NOTICE SIDEBANDS BELOW EACH TARGET SIGNAL. LARGE SPIKE IS THE ZERO FREQUENCY MARKER.

SA-1979-18

FIGURE 20 DATA DISPLAYS USED FOR REMOTE TARGET MEASUREMENTS

generate spurious target components in the beat-frequency spectrum, and since these spurious targets can introduce inaccuracies in the measurement of the relative power reflected by two targets (Figure 11), it was important to experiment with discrete targets at various ranges before tackling the distributed targets presented by plume and clear-air scattering volumes.

1. Discrete Targets

The CW lidar equipment shown in Figure 18 was used for these initial target measurements. The modulated argon laser beam was expanded to a three-inch diameter and transmitted via periscope through the roof of the laboratory and out along the target range shown in Figure 21. Also on the roof and next to the steerable output periscope mirror was the tripod-mounted lidar receiver, consisting of a 6-inch-diameter front lens, a collimating lens, and a photomultiplier tube. The mirror was adjusted to direct the beams down the parking-lot range, and the receiver was then aligned with the transmitted beam. With the laser power output reduced well below eye-safe levels, an assistant standing 90 m from the transmitter held a white card in the beam and began walking away from the lidar site. A series of photographs were taken of the spectrum analyzer's display of the difference-frequency spectrum as the target moved slowly out in range.

The spurious sideband components generated around each of the single-target returns are shown in Figure 22. The CW lidar's mixer output-frequency spectrum is displayed on a spectrum analyzer for nine target positions at successively greater ranges. Each photo presents the frequency-component amplitude on a logarithmic vertical scale versus range (beat frequency) on the horizontal. This scale tends to overemphasize the sideband strength on first impression. The large signal at

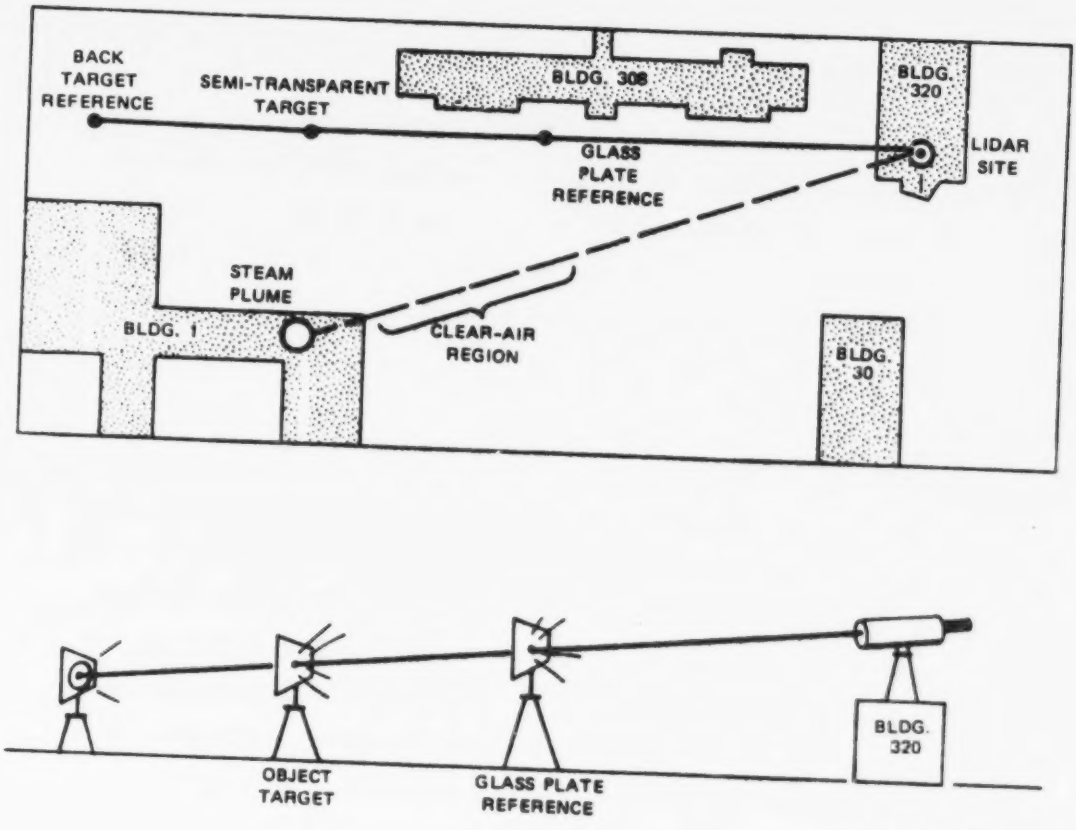

FIGURE 21 LIDAR TARGET RANGE USED FOR REMOTE RANGE AND OPACITY MEASUREMENTS

left is the zero-frequency marker generated by the spectrum analyzer. Since the sawtooth sweep repetition frequency employed is f_m = 10 kHz, the sidebands appear at multiples of 10 kHz across the display. The apparent sideband width is an artifact of the display device.

Notice in Figure 22(a) that the sidebands are approximately 20 dB below the main target component at 50 kHz. This is a result of the fact that a target located at a range node meets the minimum-sideband condition discussed in Section IV-C. In Figure 22(b) the target has moved to a range halfway between range nodes. Notice the increase in

Reproduced from best available copy.

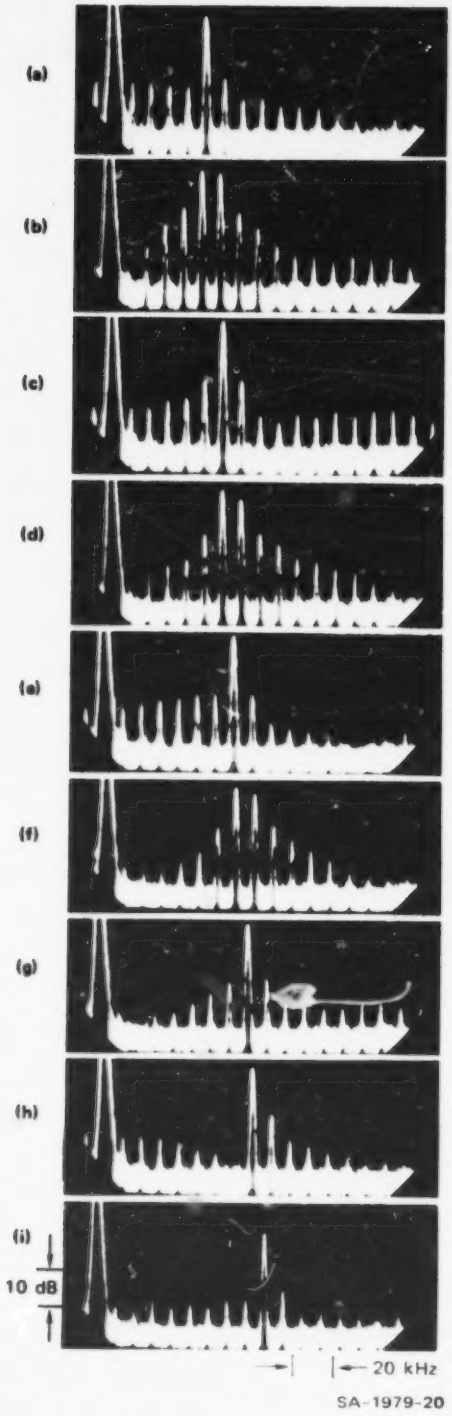

FIGURE 22 DISCRETE-TARGET SPECTRA SHOWING SPURIOUS SIDE-BAND CHANGES WITH RANGE

sideband levels. As the target moves out in range, alternate photos show the changes in the sideband power envelope for range-node locations and nonrange-node locations.

An interesting feature shown in Figure 22(h) is that just as the target moves slightly off the range-node position in 22(g), the first sideband to the left of the main target component drops below the underlying system noise level. That a particular sideband can be eliminated in this way may be a useful feature in future lidar opacimeter designs. When the clear-air signal is brought up above the system noise and the spurious sideband induced by the target is eliminated in this way, any remaining sideband amplitude will be contributed solely by energy backscattered from clear air near the target. In a real smoke-plume measurement, however, the target would not be a white card but a volume of distributed particle scatterers. A tenuous steam plume near the experimental target range provided an excellent opportunity for examining such a distributed target's characteristics when viewed by a CW lidar.

2. Steam-Plume Characteristics

Figure 21 shows the location of this steam plume near the experimental target range at SRI. Figure 23 is a photograph of the rooftop lidar site after the transmit mirror and receiver telescope had been steered over to view the steam plume. Notice that the beam's path is clearly visible due to clear-air scattering all the way through and beyond the plume. The plume itself is very reflective, and its bright front-surface reflection causes the plume target spectrum shown in Figure 24(a). Here the two plume sidebands appear approximately 10 dB below the main plume return. Additional weaker sidebands can be seen at higher frequencies, just above the system and background noise spectrum.

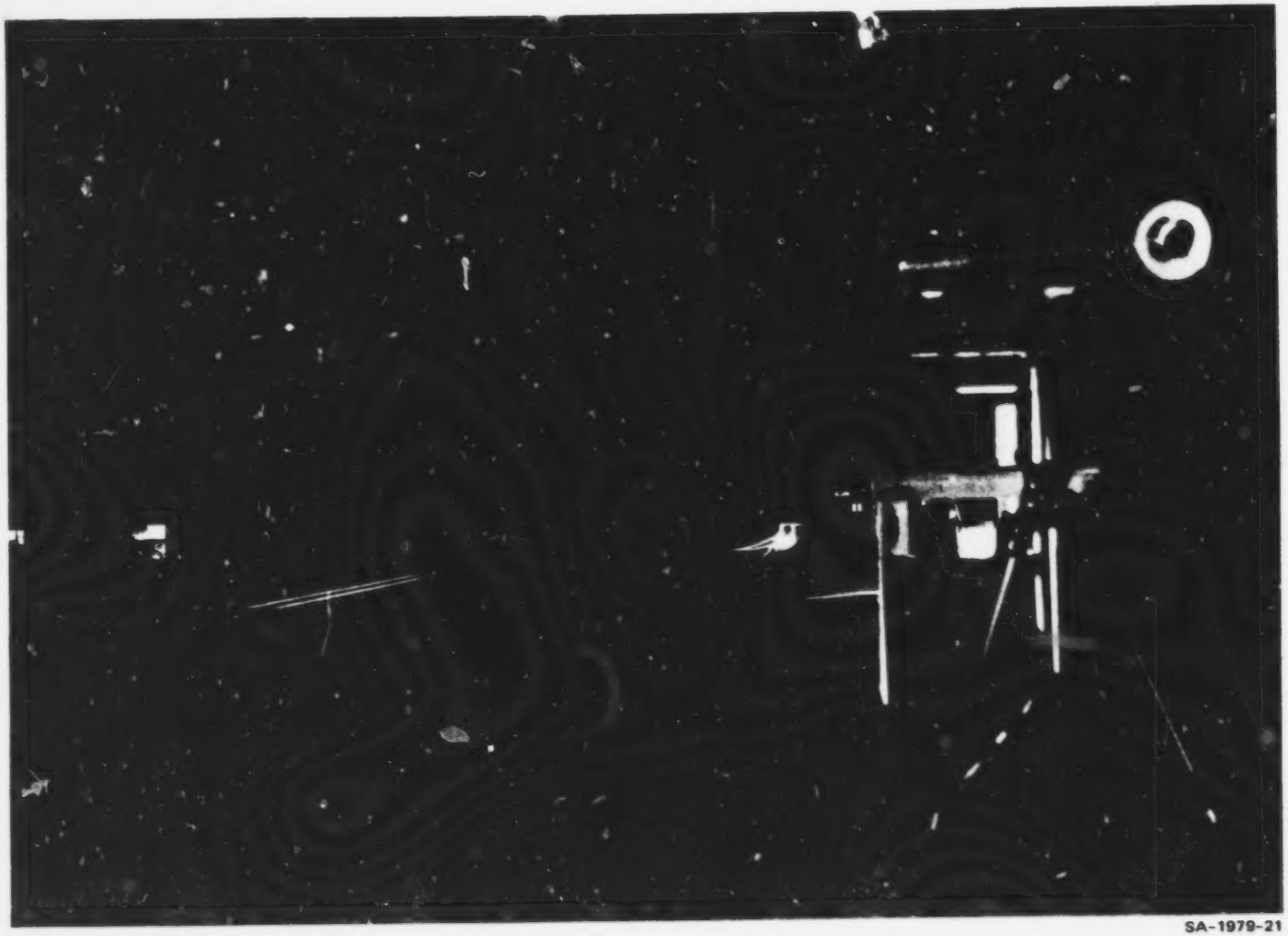

FIGURE 23 ROOFTOP LIDAR SITE

Reproduced from best available copy.

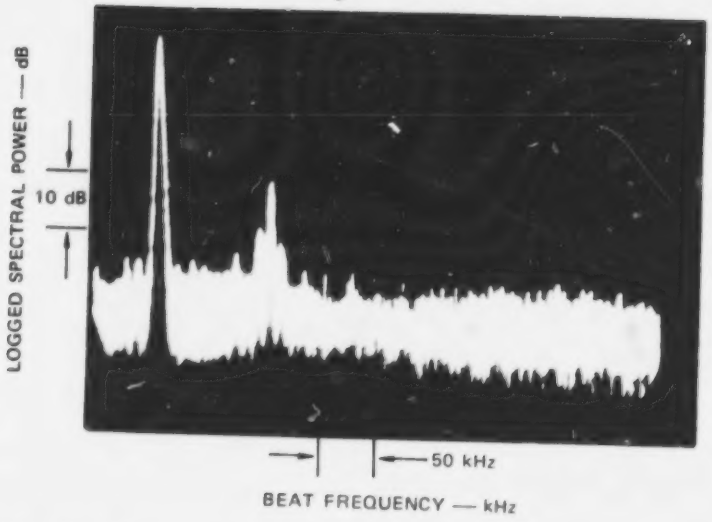

STEAM PLUME TARGET RETURN RISES ABOVE NOISE SPECTRUM BY NEARLY 20 dB. TWO LARGEST SIDEBANDS ARE 10 dB LOWER. LARGEST SPIKE IS ZERO-FREQUENCY MARKER.

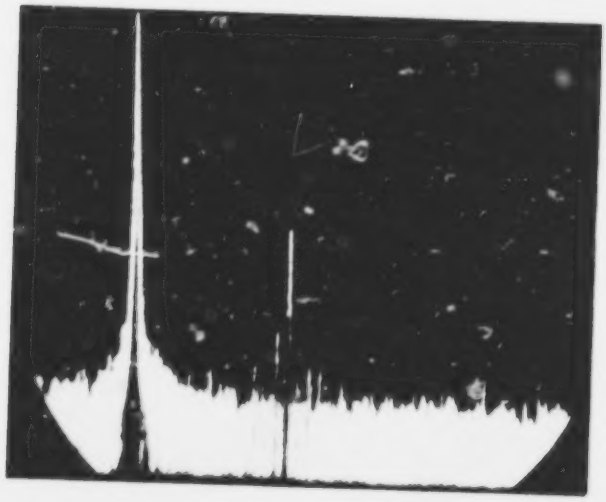

(b) SPECTRUM OF DISCRETE WALL TARGET NEAR PLUME SOURCE.

SA-1979-22

FIGURE 24 DISTRIBUTED STEAM-PLUME TARGET SPECTRUM

The steam plume return is much like a discrete target return. The moving water droplets in the plume do not appear to have caused any severe Doppler spreading in the target spectrum. Figure 24(b) is the spectrum of a discrete target--a wall--near the steam plume. The two spectra are quite similar, leading to a preliminary conclusion that multiple-scattering or Doppler effects on the beam as it passes through a plume do not make the plume target spectrum significantly different from a discrete-target display.

The detection of light scattered from clear-air regions in front of and behind the seemingly discrete plume target proved more difficult with the elementary CW lidar system built for these initial efforts. Unlike the bright return from the front surface of the plume, the backscatter from extended volumes of clear air posed a problem unique to the FM-AM-CW technique.

3. Clear-Air Targets

The primary problem in detecting clear air in the presence of a bright steam plume return was that the plume return masked the clear-air return. Since target energy appears only as spectrally narrow sidebands at multiples of f_m in the beat-frequency spectrum, the strong sideband-energy contributions from the main plume return are much greater in amplitude than the contributions by clear-air scattering. It was necessary to study the clear-air backscatter first by eliminating any bright targets other than the clear-air scatterers in the lidar's field of view.

This was done by steering the beam shown in Figure 23 off to the left of the plume. The receiver was then trained on a segment of the beam at about the range of the plume. The target spectrum of this return is shown in Figure 25(a) on a linear scale. The main target

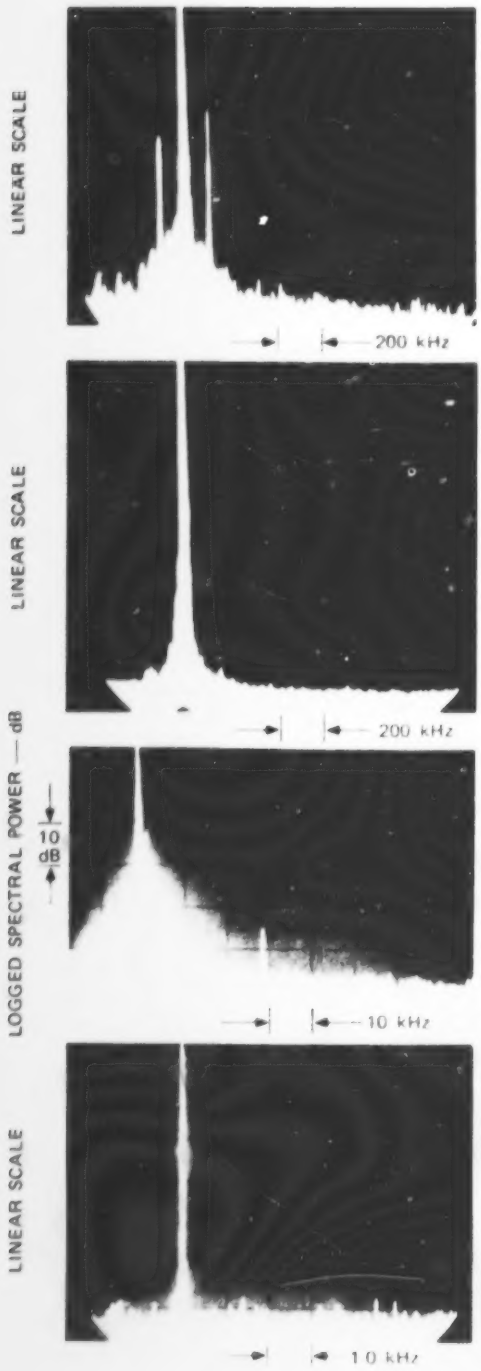

(a) MAIN-TARGET COMPONENT FROM CLEAR-AIR RETURN. LARGE SPIKE IS ZERO-FREQUENCY MARKER.
NOTICE CHANGE IN COMPONENT AMPLITUDE AS DISPLAY SWEPT FROM $-f_R$ TO $+f_R$

Reproduced from best available copy.

(b) WHEN THE LASER BEAM IS BLOCKED, THE NOISE LEVEL IS SEEN TO DROP.

c) CLEAR-AIR RETURN SIGNAL SHOWN ON LOGARITHMIC SCALE APPEARS 10 dB ABOVE NOISE. LARGE SPIKE IS ZERO-FREQUENCY MARKER.

(d) CLEAR-AIR RETURN ON EXPANDED SCALE, SHOWING THE MAIN COMPONENT IS SPECTRALLY NARROW.

SA-1979-23

FIGURE 25 CW LIDAR CLEAR-AIR RETURNS

spectral component is several times greater than the surrounding noise spectral amplitude. When the beam is blocked, the spectrum shown in Figure 25(b) results. The noise level is lower by the measure of white noise generated by PMT detection of the nonzero average intensity of the reflected beam.

On an expanded frequency scale (1 kHz/div) it can be seen that the clear-air component is spectrally narrow [Figure 25(d)]. This photo shows a spectrum scan made with a 30-Hz filter bandwidth. One can conclude that use of a similarly narrow filter to monitor the clear-air sideband center frequency will give a similar SNR better than 6:1, allowing adequate resolution of the 10-to-50 percent attenuation in the clear-air return that would be caused by an intervening smoke plume.

In order to get these clear-air returns it was necessary to narrow the receiver field of view to reduce spatial-integration effects. As discussed in Section IV-C-3, a CW lidar receiver viewing more than a fraction of the intensity modulation wavelength will suffer a loss in SNR. The series of spectrum photos in Figure 26 shows the spatial-integration effect on the SNR of the PMT output for constant field of view and increasing frequency--i.e., increasing number of modulation wavelengths in the field of view. Each photo shows the spectrum of a single modulation frequency component as detected by the PMT. As this frequency was increased, the component was recentered on the display. A similar series would result if the frequency were left constant while the receiver field of view was progressively widened.

The top photo shows a 25-dB SNR obtained from clear air when the receiver views a length of beam equal to only about 3 percent of the modulation wavelength. The following photos show how the SNR drops below 10 dB for a receiver viewing more than a full wavelength. One can reasonably conclude that spatial-integration considerations are indeed important

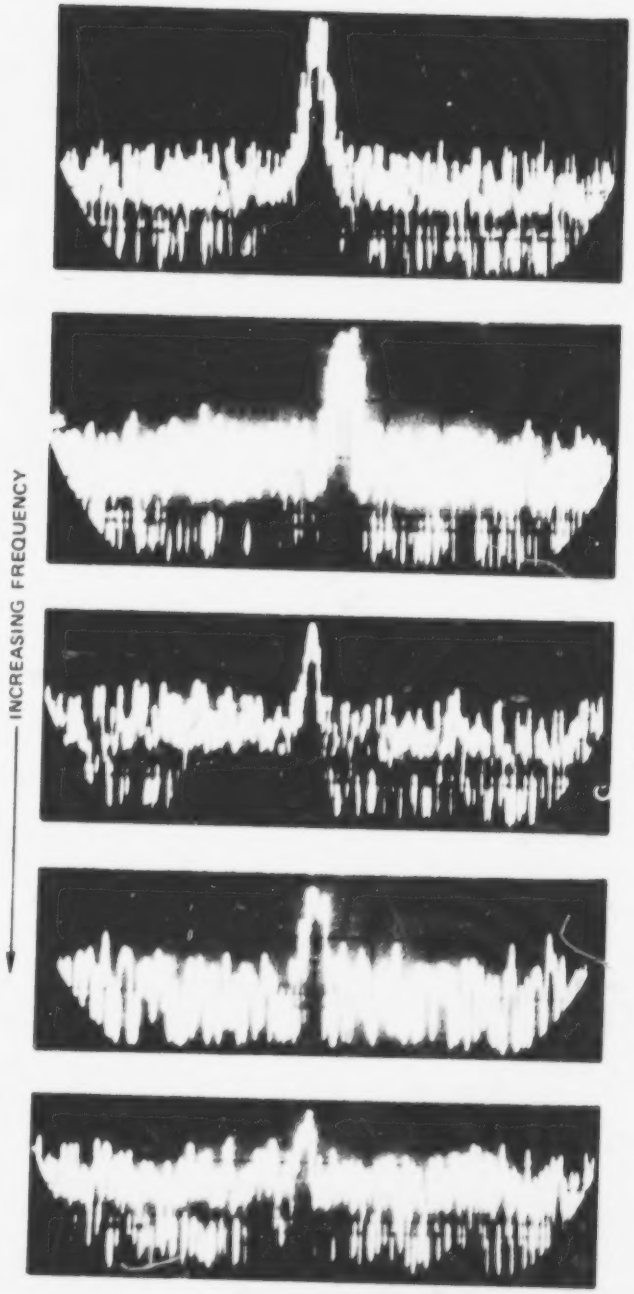

EACH PHOTO SHOWS THE SPECTRUM OF THE FREQUENCY COMPONENT USED TO MODULATE THE INTENSITY OF THE LASER BEAM, AS DETECTED BY THE PMT. AS THIS FREQUENCY IS INCREASED, IT IS RECENTERED ON THE SPECTRUM DISPLAY. SPATIAL INTEGRATION OF THE SIGNAL OVER THE CLEAR-AIR VOLUME BEING VIEWED RESULTS IN LOWER SIGNAL-TO-NOISE RATIO FOR HIGHER FREQUENCIES. FREQUENCY INCREASES FROM PHOTO TO PHOTO, MOVING DOWN THE SERIES.

SA-1979-24

FIGURE 26 EFFECTS OF SPATIAL INTEGRATION ON SIGNAL-TO-NOISE RATIO OF CLEAR-AIR RETURN

in the design of a CW lidar and in its subsequent performance in distributed-target situations.

C. Remote Opacity Measurements

Having established that a discrete target, a thin-plume target, and a clear-air volume of limited linear extent all have similar target spectra when viewed by a CW lidar, it was possible to proceed to the proof-of-principle experiments in remote measurement of lidar target opacity.

The lidar beam was again pointed downrange as shown in Figure 21. An 18-inch glass plate was placed in the beam at the fifth range-node position from zero so as to minimize its sideband-amplitude contributions at other range nodes. The plate was oriented so that its specular reflection did not return directly to the lidar receiver; instead, the receiver viewed only the diffuse scatter from the glass and dust particles on the glass. Since the glass was 90 percent transparent, most of the beam continued downrange to the ninth range-node position, where a plywood board was placed in the beam. The receiver viewed the back target through the front glass. With both targets at node ranges, their combined sideband levels were relatively low, as shown in the linear display of spectral-component amplitude versus beat frequency, Figure 27(a). It can be seen that the plywood reference target is about 1.26 times stronger than the return from the front glass reference target.

When a second glass is placed at the seventh range-node position, it adds a third component between the two reference-target components, as can be seen in Figure 27(b). The important change from 27(a) to 27(b), however, is the change in relative amplitude between the front and back reference targets. Now their ratio has been reduced to 1.02 from 1.26, meaning that the light from the back reference--passing twice through

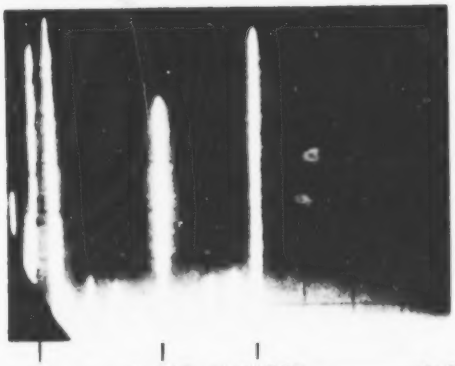

(a) FRONT GLASS REFERENCE AT FIFTH NODE RANGE AND BACK REFERENCE TARGET (plywood) AT NINTH NODE RANGE SHOWN WITH NO INTERMEDIATE SEMITRANSPARENT TARGET.

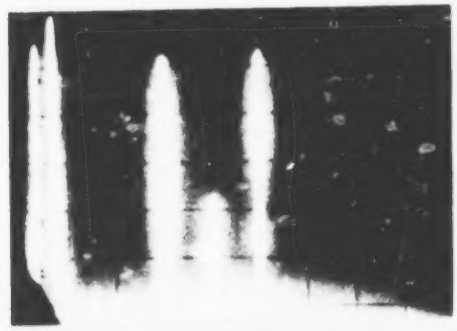

(b) INTERMEDIATE GLASS PLATE PLACED BETWEEN FIRST TWO TARGETS AT NODE-RANGE SEVEN. NOTICE THAT BACK-TARGET AMPLITUDE DROPS BY 20%, MEANING THAT ONE-WAY ATTENUATION OF GLASS PLATE IS 10%.

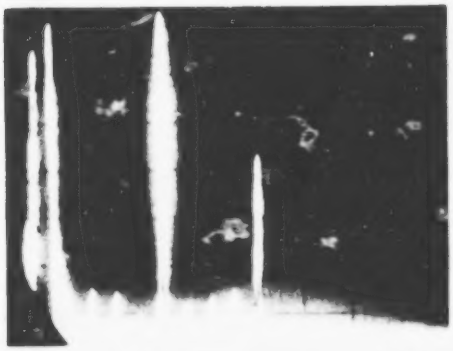

(c) ALUMINUM SCREEN REPLACES CENTER GLASS PLATE. BACK-TARGET LEVEL DROPS 43% BELOW ORIGINAL, MEANING THAT SCREEN IS 69% TRANSPARENT. THE SCREEN ITSELF DOES NOT APPEAR AS A SPIKE BECAUSE ITS REFLECTIVITY WAS MORE THAN 10 TIMES LOWER THAN THAT OF THE GLASS AND PLYWOOD.

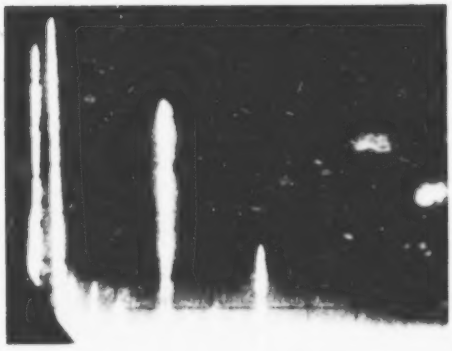

(d) FINER ALUMINUM SCREEN MESH REPLACES CENTER TARGET. FURTHER REDUCTION MEANS ONE-WAY TRANSMISSION OF 58% FOR THE FINE MESH.

SA-1979-25

FIGURE 27 CHANGES IN RELATIVE TARGET POWER LEVELS CAUSED BY VARIOUS TARGET OPACITIES

the new center target--has been attenuated to 81 percent of its intensity when only clear air lay between the references.

From this one can surmise that the two-way transmission through the center glass is 81 percent of the transmission through only the clear-air path of Figure 27(a). This corresponds to a one-way transmission of $\sqrt{0.81}$, or 90 percent, which is remarkably close to the 90 percent transmission of the plate-glass target when measured in the laboratory. Such a remote measurement of the opacity of a semitransparent target at a range of approximately 160 m was first made with this CW lidar in April 1973.

Other semitransparent center targets were measured as well. Figure 27(c) shows the spectrum for a 1/4-inch aluminum wire mesh sprayed black to reduce its reflectivity. Indeed, the return from the center target is not visible on this scale but the telltale drop in the amplitude of the return from the back reference target allows calculation of a 69 percent one-way mesh transmission. Figure 27(d) shows still further reduction when a 1/16-inch mesh is substituted in the center target position. Its transmission, calculated from the remote spectrum display, appears to be 58 percent.

More than 50 different measurements were made of the semitransparent glass and mesh targets, separately and in combination. The results of tests on these thin targets are given in Figure 28. The chart is labeled in percent transmission (one-way) and equivalent Ringelmann scale on the right. The error bars represent the range of opacity values measured for each type of target, the small dots represent the actual remotely measured value, and the large dots represent the value measured in the laboratory.

The accuracy of measurements made with this first CW lidar transmissometer was limited by a number of factors; the effects of each factor can be mitigated or eliminated by suitable refinements in technique and

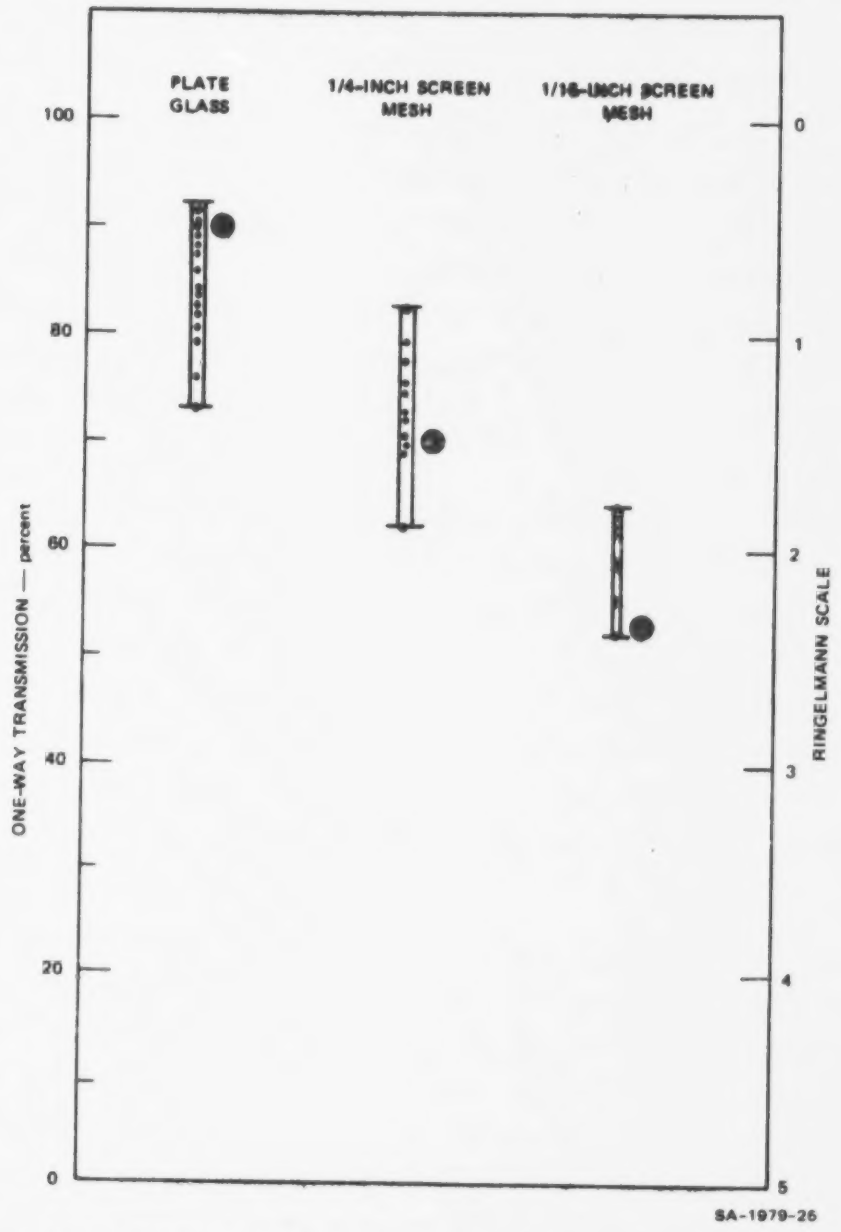

FIGURE 28 RESULTS OF REMOTE OPACITY MEASUREMENTS USING A CW LIDAR

subsequent engineering development. The most important factor was the nonlinearity of the so-called "linear" spectrum-analyzer display scale used when making three-target opacity measurements. The bottommost division on this scale can represent anywhere from 0.1 division to 1.5 divisions, depending on the signal gain taken in the spectrum analyzer's front end. Some of the extreme data points in Figure 28 result from photos taken before this equipment limitation was discovered, for which scale-correction factors were not known.

Another limiting factor was the physical nature of the reference-target setup. High winds during two experiments tended to jostle the front glass reference plate, steering its specular reflection near the receiver aperture and causing a corresponding increase in the amplitude of the front reference target. Interestingly, an operator watching the continuously refreshed target spectrum display could easily monitor this changing reference level and write off any measurements as being subject to error.

A third measurement error resulted as predicted in Figure 11. The spurious sideband generated at Node 9 by the target at Node 5 added to the amplitude of the main target component at Node 9 (and vice versa) to give an inaccurate measurement of the height of one component relative to the other.

Finally, there was the inaccuracy inherent in making centimeter-stick measurements of traces in polaroid oscilloscope photos. Earlier project plans had called for construction of a bank of three narrow-band intermediate-frequency amplifiers, each tunable to a target frequency, for continuous electronic measurement of signal amplitudes. Unfortunately, other equipment considerations required that the beat-frequency spectrum be scaled down from the 0-to-1-MHz range to the 0-to-100-kHz range. Since

the breadboard IF amplifier could not be scaled down accordingly, use of this otherwise promising signal-processing technique had to be postponed.

D. Discussion of Experimental Results

The successive milestones in this experimental study can be listed as follows:

(1) Preliminary analysis of FM-CW lidar.

(2) Design of laboratory-model lidar.

(3) Detection and ranging to discrete targets.

(4) Detection and ranging to distributed scattering targets including clear air.

(5) Remote opacity measurement using discrete object and reference targets.

(6) Proof-of-concept analysis and report.

In reaching each of these milestones, no fundamental obstacle to the use of the CW lidar was found. Every significant source of error or performance limitation was traced to an engineering technique or component that is amenable to improvement, given sufficient attention in a subsequent engineering development effort. In reviewing the results, it is unfortunate that remaining time and funds were not sufficient to accomplish a seventh milestone--namely, remote opacity measurement using the detected clear-air volumes as reference targets. In order to accomplish this milestone, an improved, low-noise PMT receiver is required, as well as a more refined signal-spectrum processor based on the three-AM-radio concept depicted in Figure 7. More realistic smoke plumes than the highly reflective steam plume used here need to be employed in testing a refined engineering model.

These are all straightforward tasks for the future. That this first hardware assembly was not quite up to reaching the ideal seventh milestone

is hardly an indictment of the technique, which passed the first six milestones in a most positive manner. It is encouraging to have learned that the atmospheric Doppler and FM-to-AM noise-conversion effects feared by theorists do not degrade system performance in practice. It was surprisingly easy to align and operate the eye-safe CW laser system, as opposed to its pulsed-laser predecessor at an equivalently early stage in its development. And it was gratifying to be able to make reasonably accurate remote measurements of target opacity between Ringelmann 0 and 1 even with the rudimentary system implementation possible within the constraints of this first-phase effort.

The principal objective of the program was successfully accomplished: the concept of CW lidar for remote opacity measurement was demonstrated along with its capacity for detecting backscatter from remote volumes of clear air. The engineering requirements for design of a subsequent engineering research model have been determined and reported.

It is concluded that the FM-AM-CW lidar technique for detection, ranging, and transmissometry through atmospheric particulates is feasible, and that straightforward improvements, primarily in receiver detector and postdetection signal processing, will allow accurate measurements of smoke plumes thinner than Ringelmann 1.

REFERENCES

1. D. W. Jackson, "Development of a CW Lidar for the Remote Measurement of Smoke-Plume Opacity," Proposal No. ELD 69-165, Stanford Research Institute, Menlo Park, California (22 January 1970).

2. W. E. Evans, "Development of Lidar Stack Effluent Opacity Measuring System," Final Report, SRI Project 6529, Stanford Research Institute, Menlo Park, California (1967).

3. W. B. Johnson, "Lidar Applications in Air Pollution Research and Control," J. Air Poll. Contr. Assoc., Vol. 19, pp. 176-180 (1969).

4. W. B. Johnson and E. E. Uthe, "Lidar Study of Stack Plumes," Final Report, Contract No. PH22-68-33 (NAPCA), SRI Project 7289, Stanford Research Institute, Menlo Park, California (1969).

5. P. M. Hamilton, "The Use of Lidar in Air Pollution Studies," Intern. J. Air and Water Poll., Vol. 10, pp. 427-434 (1966).

6. E. W. Barrett and O. Ben-Dov, "Applications of the Lidar to Air Pollution Measurements," J. Appl. Meteorol., Vol. 6, pp. 500-515 (1967).

7. W. D. Conner and J. R. Hodkinson, "A Study of the Optical Properties and Visual Effects of Smoke-Stack Plumes," Cooperative Study Project, Edison Electric Institute and U.S. Public Health Service.

8. J. E. Yocom, "Problems in Judging Plume Opacity--A Simple Device for Measuring Opacity of Wet Plumes," J. Air Poll, Control Assoc., Vol. 13, No. 1 (January 1963).

9. C. S. Cook, G. W. Bethke, and W. D. Conner, "Remote Measurement of Smoke Plume Transmittance Using Lidar," Applied Optics, Vol. 11, No. 8 (August 1972).

10. M. I. Skolnik, Introduction to Radar Systems, Section 3.3 (McGraw-Hill Book Company, San Francisco, California, 1962).

11. T. E. Honeycutt and W. F. Otto, "FM-CW Radar Range Measurement with a CO_2 Laser," IEEE J. Quantum Electronics (February 1972).

Preceding page blank

12. D. H. Sliney and B. C. Freasier, "Evaluation of Optical Radiation Hazards," Appl. Optics, Vol. 12, No. 1 (January 1973).

13. M. Ross, Laser Receivers (John Wiley and Sons, Inc., New York, New York, 1966).

14. E. T. Ebersol, "Radar Sees Gnats and Stuff!" Microwaves, p. 9 (February 1973).

15. "FM-CW Radar Detects Atmospheric Pressure," Electronic Design, Vol. 21, No. 15, p. 24 (19 July 1973).

16. A. Siegmann, Proc. IEE, pp. 1350-1356 (October 1966).